LAWRENCE
LIVERMORE
NATIONAL
LABORATORY

UCRL-JRNL-217766

7Be(p,(gamma))8B S-factor from Ab Initio No-Core Shell Model Wave Functions

P. Navratil, C. A. Bertulani, E. Caurier

December 16, 2005

Physical Review C

^{7}Be(p,γ)^{8}B S-factor from *ab initio* no-core shell model wave functions

P. Navrátil*
Lawrence Livermore National Laboratory, P.O. Box 808, L-414, Livermore, CA 94551, USA

C. A. Bertulani†
Department of Physics, University of Arizona, Tucson, AZ 85721, USA

E. Caurier‡
Institut de Recherches Subatomiques (IN2P3-CNRS-Université Louis Pasteur)
Batiment 27/1, 67037 Strasbourg Cedex 2, France

(Dated: December 15, 2005)

Nuclear structure of ^{7}Be, ^{8}B and ^{7,8}Li is studied within the *ab initio* no-core shell model (NCSM). Starting from high-precision nucleon-nucleon (NN) interactions, wave functions of ^{7}Be and ^{8}B bound states are obtained in basis spaces up to $10\hbar\Omega$ and used to calculate channel cluster form factors (overlap integrals) of the ^{8}B ground state with ^{7}Be+p. Due to the use of the harmonic oscillator (HO) basis, the overlap integrals have incorrect asymptotic properties. We fix this problem in two alternative ways. First, by a Woods-Saxon (WS) potential solution fit to the interior of the NCSM overlap integrals. Second, by a direct matching with the Whittaker function. The corrected overlap integrals are then used for the ^{7}Be(p,γ)^{8}B S-factor calculation. We study the convergence of the S-factor with respect to the NCSM HO frequency and the model space size. Our S-factor results are in agreement with recent direct measurement data. We also test the spectroscopic factors and the corrected overlap integrals from the NCSM in describing the momentum distributions in knockout reactions with ^{8}B projectiles. A good agreement with the available experimental data is also found, attesting the overall consistency of the calculations.

PACS numbers: 21.60.Cs, 21.30.Fe, 24.10.Cn, 25.40.Lw, 27.20.+n

I. INTRODUCTION

The ^{7}Be(p,γ)^{8}B capture reaction serves as an important input for understanding the solar neutrino flux [1]. Recent experiments determined the neutrino flux emitted from ^{8}B with a precision of 9% [2]. On the other hand, theoretical predictions have uncertainties of the order of 20% [3, 4]. The theoretical neutrino flux depends on the ^{7}Be(p,γ)^{8}B S-factor that needs to be known with high precision. Many experimental and theoretical investigations were devoted to this reaction. Experiments were performed using direct measurement techniques with proton beam and ^{7}Be targets [5–7] as well as by indirect methods when a ^{8}B beam breaks up into ^{7}Be and proton in the Coulomb field of a heavy target [8, 9]. Theoretical calculations needed to extrapolate the measured S-factor to the astrophysically relevant Gamow energy were performed with several methods: the R-matrix parametrization [10], the potential model [11–13], and the microscopic cluster models [14–16].

In this work, we present the first calculation of the ^{7}Be(p,γ)^{8}B S-factor starting from the *ab initio* wave functions of ^{8}B and ^{7}Be. We apply the *ab initio* no-core shell model (NCSM) [17, 18]. In this method, one considers nucleons interacting by high-precision nucleon-nucleon (NN) potentials. There are no adjustable or fitted parameters. Within the NCSM, we study the binding energies and other nuclear structure properties of ^{7}Be, ^{8}B as well as ^{7,8}Li, and calculate overlap integrals for the ^{8}B and ^{7}Be bound states. Due to the use of the harmonic-oscillator (HO) basis, we have to correct the asymptotic behavior of the NCSM overlap integrals. This is done in two alternative ways. First, by fitting Woods-Saxon (WS) potential solutions to the interior part of the NCSM overlap integrals under the constraint that the experimental ^{7}Be+p threshold is reproduced. Second, by a direct matching of the NCSM overlap integrals and the Whittaker function. The corrected overlap integrals are then utilized to calculate the ^{7}Be(p,γ)^{8}B S-factor as well as momentum distributions in stripping reactions. We pay special attention to the convergence of the S-factor with respect to the NCSM model space size and the HO frequency.

In Sect. II, we present the NCSM results for ^{7}Be, ^{8}B and ^{7,8}Li energies, ground-state radii and electromagnetic moments and transitions. The calculation of cluster form factors and the correction of their asymptotics is described in Sect. III. A test of the corrected NCSM overlaps and spectroscopic factors for the momentum distributions in the stripping reaction $(^7\mathrm{Be} + p) + A \longrightarrow {}^7\mathrm{Be} + X$ is discussed in Sect. IV. The S-factor calculation with sensitivity and convergence studies is presented in Sect. V. Conclusions are drawn in Sect. VI.

*navratil1@llnl.gov
†bertulani@physics.arizona.edu
‡etienne.caurier@ires.in2p3.fr

II. NUCLEAR STRUCTURE OF ^{7}BE, ^{7}LI, ^{8}B AND ^{8}LI

A. *Ab initio* no-core shell model

In the NCSM, we consider a system of A point-like non-relativistic nucleons that interact by realistic two- or two- plus three-nucleon interactions. The calculations are performed using a finite harmonic oscillator (HO) basis. As in the present application we aim at describing loosely bound states, it is desirable to include as many terms as possible in the expansion of the total wave function. By restricting our study to two-nucleon (NN) interactions, even though the NCSM allows for the inclusion of three-body forces [19], we are able to maximize the model space and to better observe the convergence of our results. The NCSM theory was outlined in many papers. Here, we only briefly review the main points for the case when the Hamiltonian is restricted to just a two-nucleon interaction.

We start from the intrinsic two-body Hamiltonian for the A-nucleon system $H_A = T_{rel} + \mathcal{V}$, where T_{rel} is the relative kinetic energy and $\mathcal{V}$ is the sum of two-body nuclear and Coulomb interactions. Since we solve the many-body problem in a finite HO basis space, it is necessary that we derive a model-space dependent effective Hamiltonian. For this purpose, we perform a unitary transformation [17, 18, 20, 21] of the Hamiltonian, which accommodates the short-range correlations. In general, the transformed Hamiltonian is an A-body operator. Our simplest, yet non-trivial, approximation is to develop a two-particle cluster effective Hamiltonian, while the next improvement is to include three-particle clusters, and so on. The effective interaction is then obtained from the decoupling condition between the model space and the excluded space for the two-nucleon transformed Hamiltonian. Details of the procedure are described in Refs. [17, 18]. The resulting two-body effective Hamiltonian depends on the nucleon number A, the HO frequency Ω, and $N_{\max}$, the maximum many-body HO excitation energy defining the model space. It follows that the effective interaction approaches the starting bare interaction for $N_{\max} \to \infty$. Our effective interaction is translationally invariant. A significant consequence of this fact is the factorization of our wave functions into a product of a center-of-mass $\frac{3}{2}\hbar\Omega$ component times an internal component.

Our most significant approximation here is the use of the two-body cluster approximation to the effective many-body Hamiltonian. Our method is not variational so higher-order terms may contribute with either sign to total binding. Hence, evaluating the dependence on the basis-space parameters help calibrate our convergence.

Once the effective interaction is derived, we diagonalize the effective Hamiltonian in a Slater determinant HO basis that spans a complete $N_{\max}\hbar\Omega$ space. This is a highly non-trivial problem due to very large dimensions we encounter. To solve this problem we have used a specialized version of the shell model code Antoine [22, 23], recently adapted to the NCSM [24, 25]. This code works in the M scheme for basis states, and uses the Lanczos algorithm for diagonalization. Its basic idea is to write the basis states as a product of two Slater determinants, a proton one and a neutron one. Matrix elements of operators are calculated for each separate subspace (one-body for the proton-neutron, two-body for the proton-proton and neutron-neutron). The performance of the code is the best when the ratio between the number of proton plus neutron Slater determinants and the dimension of the matrix is the least. It happens when the number of proton Slater determinants is equal the number of the neutron Slater determinants. The number of iterations needed to converge the first eigenstates is significantly reduced by the implementation of a sophisticated strategy for selecting the pivot vectors. The difficulty of the no-core calculations (in which all nucleons are active) is that the number of shells and, consequently, the number of matrix elements that are precalculated, becomes very large. One has to handle a huge number of operators. This is the reason why it has been necessary to write a specialized version of the code.

A recent development of the NCSM is the ability to further process the wave functions, resulting from the shell-model calculation, to obtain channel cluster form factors [26] and, consequently, the spectroscopic factors.

B. Nucleon-nucleon interactions

Two different, high-precision NN interactions have been used in this study: the CD-Bonn 2000 [27] and the INOY (Inside Nonlocal Outside Yukawa) [28, 29] potentials.

The CD-Bonn 2000 potential [27] as well as its earlier version [30] is a charge-dependent NN interaction based on one-boson exchange. It is described in terms of covariant Feynman amplitudes, which are non-local. Consequently, the off-shell behavior of the CD-Bonn interaction differs from local potentials which leads to larger binding energies in nuclear few-body systems.

A new type of interaction, which respects the local behavior of traditional NN interactions at longer ranges but exhibits a non-locality at shorter distances, was recently proposed by Doleschall *et al.* [28, 29]. The authors explore the extent to which effects of multi-nucleon forces can be absorbed by non-local terms in the NN interaction. Their goal was to investigate if it is possible to introduce non-locality in the NN interaction so that it correctly describes the three-nucleon bound states ^{3}H and ^{3}He, while still reproducing NN scattering data with high precision. The so called IS version of this interaction, introduced in Ref. [28], contains short-range non-local potentials in $^1S_0$ and $^3S_1 - {}^3D_1$ partial waves while higher partial waves are taken from Argonne v_{18}. In this study we are using the IS-M version, which includes non-local potentials also in the P and D waves [29]. It is important to note that, for this particular version, the

on-shell properties of the triplet P-wave interactions have been modified in order to improve the description of $3N$ analyzing powers. The $^3P_0$ interaction was adjusted to become less attractive, the $^3P_1$ became more repulsive, and the $^3P_2$ more attractive. Unfortunately, this gives a slightly worse fit to the Nijmegen ^3P phase shifts.

C. ^{7}Be and ^{7}Li

Our calculations for both $A = 7$ and $A = 8$ nuclei were performed in model spaces up to $10\hbar\Omega$ for a wide range of HO frequencies. We then selected the optimal HO frequency corresponding to the ground-state energy minimum in the $10\hbar\Omega$ space and performed a $12\hbar\Omega$ calculation to obtain the ground-state energy and the point-nucleon root-mean-square (rms) radii. The overlap integrals as well as other observables were, however, calculated only using wave functions from up to $10\hbar\Omega$ spaces.

The ^{7}Be ground-state energy dependence on the HO frequency for different model spaces is shown in Figs. 1 and 2 for the CD-Bonn 2000 and the INOY NN potentials, respectively. We observe a quite different convergence trend for the two potentials. For the INOY, the convergence is very uniform with respect to the HO frequency with substantial changes with $N_{\max}$. The convergence with increasing $N_{\max}$ is evident as also seen in the inset of the Fig. 2. It is straightforward to extrapolate that the converged INOY ground-state energy will slightly overbind ^{7}Be. The ground-state energy convergence for the CD-Bonn is quite different with a stronger dependence on the frequency, with minima shifting to smaller frequency with basis size increase, and an overall weaker dependence on $N_{\max}$. Contrary to the INOY, the CD-Bonn underbinds ^{7}Be by more than 3 MeV, which is typical for the standard high-precision NN potentials.

From these results we select the optimal frequency $\hbar\Omega = 12$ MeV for the CD-Bonn 2000 and $\hbar\Omega = 16$ MeV for the INOY potential. Corresponding spectra obtained using these frequencies are then shown in Figs. 3 and 4. The energies, radii and electromagnetic observables are summarized in Tables I and II, where we also include the ^{7}Li results. We obtain the same level ordering for ^{7}Be and ^{7}Li which is also the same for both NN potentials with the exception of a reversal of the $7/2^-_2$ and $1/2^-_2$ levels. Our CD-Bonn ordering is in agreement with experiment for the 9 lowest levels in ^{7}Li. In ^{7}Be, the experimental $7/2^-_2$ and $3/2^-_2$ levels are reversed compared to our results and the situation in ^{7}Li. Our calculated spectra show a good convergence with the basis size enlargement as well as a good stability with respect to the frequency change. An interesting feature is a different level spacing of the $7/2^-_1$, $5/2^-_1$ and $5/2^-_2$ levels for the CD-Bonn and INOY calculations. The INOY results are similar to those obtained when a three-body interaction is included in the Hamiltonian [19]. This is not surprising as discussed in Subsect. II B.

Concerning the magnetic moments and M1 transitions, we can see a very little dependence of the calculated values on the HO frequency or the basis size. Also the two NN potentials give very similar results that are in a reasonable agreement with experiment. Concerning the radii and quadrupole moments, the calculated values in general increase with increasing basis size and decreasing frequency. This is in part a consequence of the incorrect asymptotics of the HO basis. The fastest convergence for the radii and quadrupole moment occurs at a smaller HO frequency. In the CD-Bonn calculations for $\hbar\Omega = 11$ and 12 MeV, the radii are close to experimental values. The quadrupole moments are still underestimated. For the INOY potential we observe underestimation of both radii and quadrupole moments. This is not unexpected as the INOY NN potential also underpredicts the ^{4}He radius.

D. ^{8}B and ^{8}Li

Our ^{8}B ground-state energy results are presented in Figs. 5 and 6 as well as in Table III where we also show the excitation energies and the corresponding ^{8}Li results. The basis size dependence of the ^{8}B spectra calculated using the optimal HO frequencies is shown in Figs. 7 and 8 for the CD-Bonn and INOY NN potentials, respectively. Similar conclusions can be drawn as for the $A = 7$ nuclei concerning convergence. The INOY NN potential gives binding energy close to the experimental one and a small overbinding is expected based on extrapolation of our $N_{\max}$ dependence. The CD-Bonn underbinds both ^{8}B and ^{8}Li by about 5 MeV. We note that the $A = 8$ nuclei, with emphasis on ^{8}Be, were also investigated within the NCSM in Ref. [24]. The present ^{8}B and ^{8}Li CD-Bonn binding energy results are basically identical to those of Ref. [24] with small differences due to the use of different versions, [27] vs. [30], of the CD-Bonn NN potential. It is interesting to note that both employed NN potentials predict ^{8}B unbound, contrary to experiment. The problem is less severe for the INOY NN potential. This suggests that a three-nucleon interaction is essential to reproduce the experimental threshold. This may appear as a problem in view of the present application to ^{7}Be(p,γ)^{8}B reaction. However, since our basis has incorrect asymptotics in the first place, we make use of only the interior part of our *ab initio* wave functions that are presumably unaffected by the wrong threshold placements. This is discussed in the next section.

Concerning the ground-state energy systematics of the $A = 7$ and $A = 8$ nuclei, we note that recent Green's function Monte Carlo (GFMC) calculations for ^{7}Li and ^{8}Li using the Argonne potentials [33] found qualitatively similar differences between the calculated and experimental values as we observe here.

Concerning the excitation energies, a noticeable difference between the CD-Bonn and the INOY predictions for the low-lying levels is a reversed order of the 0^+_1 and 3^+_1 states. We note, however, that the 0^+_1 state has not been

observed experimentally.

As seen from Table IV, the radii and quadrupole moments are substantially larger and closer to experiment in our CD-Bonn calculations. Contrary to the ^{7}Be-^{7}Li case, here we observe an interesting difference between the two NN potentials for the magnetic moment prediction. The INOY NN potential gives the magnetic moment of ^{8}Li greater than that of ^{8}B in agreement with experiment, while the CD-Bonn predicts the opposite. Interestingly, almost identical ^{8}Li and ^{8}B magnetic moments as we obtained using the CD-Bonn were reported in Ref. [16] calculated within a cluster model applied to the ^{7}Be(p,γ)^{8}B reaction. Clearly, our results suggest that the $A = 8$ magnetic moments are sensitive to a presence of three-nucleon interaction in the Hamiltonian (that is mocked up to certain degree by the INOY NN potential). As to the B(M1;$1^+ \rightarrow 2^+$) transition, both potentials gives about the same result that is in agreement with the ^{8}Li experimental value but by almost a factor of three smaller than the experimental value for ^{8}B. We note the large experimental error bar of the latter. It appears that the ^{8}B experimental values is inconsistent with both the analogous ^{8}Li value and our calculations.

III. CLUSTER FORM FACTORS FROM *AB INITIO* WAVE FUNCTIONS

A. Overlap functions and spectroscopic factors obtained in the model space

Detailed knowledge of nuclear structure is important for the description of low-energy nuclear reactions. As the first step in the application of the NCSM to low-energy nuclear reactions, one needs to understand the cluster structure of the eigenstates. This is achieved by calculating the channel cluster form factors (or overlap integrals, overlap functions). The formalism for calculating the channel cluster form factors from the NCSM wave functions was developed in Ref. [26]. Here we just briefly repeat and adapt a part of the formalism relevant for our present application.

We consider a composite system of A nucleons, i.e. ^{8}B, a nucleon projectile, here a proton, and an $A-1$-nucleon target, i.e. ^{7}Be. Both nuclei are assumed to be described by eigenstates of the NCSM effective Hamiltonians expanded in the HO basis with identical HO frequency and the same (for the eigenstates of the same parity) or differing by one unit of the HO excitation (for the eigenstates of opposite parity) definitions of the model space. The target and the composite system is assumed to be described by wave functions expanded in Slater determinant single-particle HO basis (that is obtained from a calculation using a shell model code like Antoine).

Let us introduce a projectile-target wave function

$$\begin{aligned}
&\langle \vec{\xi}_1 \dots \vec{\xi}_{A-2} r' \hat{r} | \Phi^{(A-1,1)JM}_{(l\frac{1}{2})j;\alpha I_1}; \delta_r \rangle \\
&= \sum (jmI_1M_1|JM)(lm_l\tfrac{1}{2}m_s|jm)\tfrac{\delta(r-r')}{rr'} \\
&\times\ Y_{lm_l}(\hat{r})\chi_{m_s}\langle \vec{\xi}_1 \dots \vec{\xi}_{A-2}|A-1\alpha I_1 M_1\rangle \ , \qquad (1)
\end{aligned}$$

where $\langle \vec{\xi}_1 \dots \vec{\xi}_{A-2}|A-1\alpha I_1 M_1\rangle$ and χ_{m_s} are the target and the nucleon wave function, respectively. Here, l is the channel relative orbital angular momentum, $\vec{\xi}$ are the target Jacobi coordinates and $\vec{r} = \left[\frac{1}{A-1}(\vec{r}_1 + \vec{r}_2 + \dots + \vec{r}_{A-1}) - \vec{r}_A\right]$ describes the relative distance between the nucleon and the center of mass of the target. The spin and isospin coordinates were omitted for simplicity.

The channel cluster form factor is then defined by

$$g^{A\lambda J}_{(l\frac{1}{2})j;A-1\alpha I_1}(r) = \langle A\lambda J|\mathcal{A}\Phi^{(A-1,1)J}_{(l\frac{1}{2})j;\alpha I_1}; \delta_r\rangle \ , \qquad (2)$$

with $\mathcal{A}$ the antisymmetrizer and $|A\lambda J\rangle$ an eigenstate of the A-nucleon composite system (here ^{8}B). It can be calculated from the NCSM eigenstates obtained in the Slater-determinant basis from a reduced matrix element of the creation operator:

$$\begin{aligned}
\langle A\lambda J|\ \mathcal{A}\ \Phi^{(A-1,1)J}_{(l\frac{1}{2},j);\alpha I_1}; \delta_r\rangle &= \sum_n R_{nl}(r) \\
&\times\ \frac{1}{\langle nl00l|00nll\rangle_{\frac{1}{A-1}}}\frac{1}{\hat{J}}(-1)^{I_1-J-j} \\
&\times\ {}_{\rm SD}\langle A\lambda J||a^\dagger_{nlj}||A-1\alpha I_1\rangle_{\rm SD} \ . \qquad (3)
\end{aligned}$$

The subscript SD refers to the fact that these states were obtained in the Slater determinant basis, i.e. by using a shell model code, and, consequently, contain spurious center-of-mass components. A general HO bracket, which value is simply given by

$$\langle nl00l|00nll\rangle_{\frac{1}{A-1}} = (-1)^l\left(\frac{A-1}{A}\right)^{\frac{2n+l}{2}} \ , \qquad (4)$$

then appears in Eq. (3) in order to remove these components. The $R_{nl}(r)$ in Eq. (3) is the radial HO wave function with the oscillator length parameter $b = \sqrt{\frac{\hbar}{\frac{A-1}{A}m\Omega}}$, where m is the nucleon mass.

A conventional spectroscopic factor is obtained by integrating the square of the cluster form factor:

$$S^{A\lambda J}_{(l\frac{1}{2})j;A-1\alpha I_1} = \int dr r^2 |g^{A\lambda J}_{(l\frac{1}{2})j;A-1\alpha I_1}(r)|^2 \ . \qquad (5)$$

We calculated the $\langle^8$B$|^7$Be+p$\rangle$ channel cluster form factors and the spectroscopic factors for the bound states of ^{8}B and ^{7}Be from the NCSM wave functions obtained in model spaces up to $N_{\rm max} = 10$ ($10\hbar\Omega$) in a wide HO frequency range and using both the CD-Bonn and the INOY NN potentials. The most important channels are

the p-waves, $l = 1$, with the proton in the $j = 3/2$ and $j = 1/2$ states. Our selected spectroscopic factor results are summarized in Table V. It should be noted a very weak dependence of the spectroscopic factors on either the basis size or the HO frequency or the NN potential.

We note that the $\langle^8\text{Li}|^7\text{Li+n}\rangle$ spectroscopic factors were obtained from ^{7}Li(d,p)^{8}Li stripping measurements through a distorted-wave Born approximation (DWBA) analysis [34, 35]. The NCSM $\langle^8\text{Li}|^7\text{Li+n}\rangle$ and $\langle^8\text{B}|^7\text{Be+p}\rangle$ spectroscopic factors are almost identical and overestimate those extracted in Ref. [34, 35] with the ground-state values of about 0.9. At the same time, the NCSM spectroscopic factors are in good agreement with those obtained in R-matrix analysis by Barker [10]. Also, they are consistent with the spectroscopic factors from the microscopic three-cluster model [16] as well as with the Cohen-Kurath spectroscopic factors [36] with no center-of-mass correction.

B. Correction of the overlap-function asymptotics

The dominant p-wave $j = 3/2$ overlap integral for the ^{8}B and ^{7}Be ground states obtained using the CD-Bonn NN potential in the $10\hbar\Omega$ model space and the HO frequency of $\hbar\Omega = 12$ MeV is presented in Fig. 9 by the full line. Despite the fact that a very large basis was employed in the present calculation, it is apparent that the overlap integral is nearly zero at about 10 fm. This is a consequence of the HO basis asymptotics. A separate issue is the incorrect threshold placements obtained from the high precision NN potentials that we employ. The proton capture on ^{7}Be to the weakly bound ground state of ^{8}B associated dominantly by the $E1$ radiation is a peripheral process. Consequently, the overlap integral with an incorrect asymptotic behavior cannot be used to calculate the S-factor.

It is our expectation, however, that the interior part of the overlap integral as obtained from our large-basis NCSM calculation is realistic. This is supported by the fact that the overlap integrals obtained using the CD-Bonn 2000 and the INOY NN potentials are similar despite the fact that the two potentials predict different binding energies and thresholds. Further, we calculated overlap integrals using a Hamiltonian that included the three-nucleon interaction. In those calculations, for technical reasons limited to small model spaces up to $6\hbar\Omega$, we obtained binding energies closer to experiment. Still, the interior part of the overlap integrals was almost the same as that calculated here from the CD-Bonn 2000 in the same model space and identical HO frequency. It is then straightforward to correct the asymptotic behavior of the overlap integral and fix in this way both the HO basis and the wrong threshold placement issues at the same time. One possibility we explored utilizes solutions of a Woods-Saxon potential. In particular, we performed a least-square fit of a WS potential solution to the interior of the NCSM overlap in the range of $0 - 4$ fm. The WS potential parameters were varied in the fit under the constraint that the experimental separation energy of ^{7}Be+p, i.e. 0.137 MeV, was reproduced. In this way we obtain a perfect fit to the interior of the overlap integral and a correct asymptotic behavior at the same time. The resulting overlap function is presented in Fig. 9 by the dashed line.

Another possibility is a direct matching of logarithmic derivatives of the NCSM overlap integral and the Whittaker function:

$$\frac{d}{dr} ln(r g_{lj}(r)) = \frac{d}{dr} ln(C_{lj} W_{-\eta,l+1/2}(2k_0 r)) \ , \qquad (6)$$

where η is the Sommerfeld parameter, $k_0 = \sqrt{2\mu E_0}/\hbar$ with μ the reduced mass and E_0 the separation energy (here $E_0 = 0.137$ MeV). The NCSM overlap integral $g_{lj}(r)$ is defined in Eq. (2), and, according to Eq. (3), it is expanded in terms of the HO radial wave functions, i.e. $r g_{lj}(r) = \sum_n s_{nlj} \mathcal{R}_{nl}(r)$ with $\mathcal{R}_{nl}(r) = r R_{nl}(r)$. The spectroscopic factor (5) is then given by $S_{lj} = \sum_n s^2_{nlj}$. For simplicity, we suppressed all quantum numbers except the orbital momentum l, the total proton angular momentum j and the radial HO quantum number n. With the help of

$$\begin{aligned} \frac{d}{dr}\mathcal{R}_{nl}(r) \ &= \ \left(\frac{2n+l+1}{r} - \frac{r}{b^2}\right)\mathcal{R}_{nl}(r) \\ &\quad -\sqrt{n(n+l+\tfrac{1}{2})}\frac{2}{r}\mathcal{R}_{n-1l}(r) \ , \end{aligned} \qquad (7)$$

it is straightforward to calculate the derivative of $r g_{lj}(r)$. Since asymptotic normalization constant (ANC) C_{lj} cancels out, there is a unique solution of Eq. (6) at $r = R_m$. For the discussed overlap presented in Fig. 9, we found $R_m = 4.05$ fm. Finally, by matching the value of the NCSM overlap and the Whittaker function at R_m, we determine the ANC. The corrected overlap using the Whittaker function matching is shown in Fig. 9 by a dotted line. In general, we observe that the approach using the WS fit leads to deviations from the original NCSM overlap starting at a smaller radius. In addition, the WS solution fit introduces an intermediate range from about 4 fm to about 6 fm, where the corrected overlap deviates from both the original NCSM overlap and the Whittaker function. Perhaps, this is a more realistic situation compared to the direct Whittaker function matching. In any case, by considering the two alternative procedures we are in a better position to estimate uncertainties in our S-factor results. This is discussed later.

In the end, we re-scale the corrected overlap functions to preserve the original NCSM spectroscopic factor (given in Table V). In general, we observe a faster convergence of the spectroscopic factors than that of the overlap functions. With increasing basis size ($N_{\max}$), the maximum of the overlap functions decreases while the tail extends with the integral of the square approximately conserved. This is demonstrated in Fig. 10, see further discussion below. The corrected overlap function should represent

the infinite space result. By re-scaling a corrected overlap function obtained at a finite $N_{\max}$, we approach faster the infinite space result.

The same procedure is applied to other relevant channels. In Fig. 11, we present the NCSM overlap integral and its corrected form for the other p-wave channel with proton in $j = \frac{1}{2}$ and ^{8}B and ^{7}Be in their ground states. Obviously, the WS parameters as well as the matching radii R_m obtained for the two channels are different (in the case of the present $j = \frac{1}{2}$ channel we found $R_m = 4.23$ fm). In Table VI, we show the fitted WS potential parameters obtained in the two discussed cases together with parameters corresponding to a p-wave channel with ^{7}Be in the first excited state. In this last case, the separation energy is $E_0 = 0.57$ MeV. We use the definition of the WS potential as given, e.g. in Eqs. (5-7) of Ref. [37]. Typically, the central potential parameters R_0, a_0 are well constrained in the fit, while the spin-orbit potential parameters are obtained with some uncertainty. Their values then exhibit more variation from channel to channel. The strength of the central potential V_0 was re-adjusted at every step during the fit to reproduce the experimental separation energy. We note that parameter values in Table VI are rounded compared to the results from our fitting procedure. One needs to fine-tune, e.g. the V_0, to reproduce accurately the respective separation energy in order to use the parameters independently.

It should be noted that the Woods-Saxon potential here is just a tool to represent the interior part of the NCSM overlap integral as accurately as possible and correct its asymptotic form at the same time. The range used in the least-square fit is not arbitrary and varies from channel to channel. The aim is to use as large range as possible, while at the same time preserve the NCSM overlap integral as accurately as possible in that range. A combination of eye-guided evaluation with a quantitative condition of minimizing the least-square function per fitted point helps to determine the largest possible range. Finally, let us repeat that the alternative procedure of the direct Whittaker function matching is completely unique.

The corrected overlap integrals then serve as the input for the momentum distribution and the S-factor calculations as described in the following sections.

The basis size dependence of the overlap integrals both the original NCSM and the corrected ones (using the WS solution fit procedure) can be judged from Fig. 10, where we compare results obtained in model spaces from $6\hbar\Omega$ to $10\hbar\Omega$ using the CD-Bonn 2000 NN potential and a fixed HO frequency of $\hbar\Omega = 12$ MeV. With an increase of the basis, the maximum of the overlap decreases and its tail extends to larger distances. The corresponding spectroscopic factors differ very little, see Table V. The change from $8\hbar\Omega$ to $10\hbar\Omega$ is smaller than that between $6\hbar\Omega$ and $8\hbar\Omega$, a sign of convergence. In Fig. 12, we then compare the overlap integrals, both original and corrected, obtained in the $10\hbar\Omega$ model space using three different HO frequencies. With a decrease of the HO frequency, the maximum of the overlap decreases and shifts to a larger distance. At the same time, the tail extends to larger distances as well. Finally, in Fig. 13 we compare overlap integrals obtained using the CD-Bonn 2000 and the INOY NN potentials in the same $10\hbar\Omega$ model spaces and the same HO frequency of $\hbar\Omega = 14$ MeV. While the spectroscopic factors are almost identical, the CD-Bonn overlap integral has a smaller maximum shifted to a larger distance and also extends further. The parameters of the WS potential that produce the INOY corrected overlap integral are given in Table VI. The impact of these discussed dependencies on the ^{7}Be(p,γ)^{8}B S-factor is discussed in Sect. V.

IV. MOMENTUM DISTRIBUTIONS

The stripping reaction $(^7\mathrm{Be} + p) + A \longrightarrow {}^7\mathrm{Be} + X$ cross section, for a specified final state of the core (^{7}Be), is given by [39] (for more details, see Ref. [40])

$$\frac{d\sigma_{\rm str}}{d^3k_c} = \frac{1}{(2\pi)^3}\frac{1}{2l_b+1}\sum_{m_b}\int d^2b_p\left[1-|S_p\left(b_p\right)|^2\right] \times \left|\int d^3r\; e^{-i\mathbf{k}_c.\mathbf{r}} S_c\left(b_c\right) g^{A\lambda J_b}_{(l_b\frac{1}{2})j_b;A-1\alpha I_1}(r) Y_{l_b m_b}(\hat{\mathbf{r}})\right|^2 \quad (8)$$

where $\mathbf{r} \equiv (r,\theta,\phi) \equiv (\rho,z,\phi) = \mathbf{r}_p - \mathbf{r}_c$. S_c (S_p) are the S-matrices for the core(^{7}Be)+target and the proton+target scattering, respectively. The overlap integral $g^{A\lambda J_b}_{(l_b\frac{1}{2})j_b;A-1\alpha I_1}(r)$ describing the bound state of the $(^7\mathrm{Be}+\mathrm{p})$ subsystem is defined as in Eq. (2) with its asymptotic tail corrected as described in Sect. III B.

The cross sections for the longitudinal momentum distributions are obtained by integrating Eq. (8) over the transverse component of $\mathbf{k}_c$, i.e.

$$\frac{d\sigma_{\rm str}}{dk_z} = \frac{1}{2\pi}\frac{1}{2l_b+1}\sum_{m_b}\int d^2b_p\left[1-|S_p\left(b_p\right)|^2\right] \times \int d^2\rho\,|S_c\left(b_c\right)|^2 \times \left|\int_{-\infty}^{\infty} dz \exp\left[-ik_z z\right] g^{A\lambda J_b}_{(l_b\frac{1}{2})j_b;A-1\alpha I_1}(r) Y_{l_b m_b}(\hat{\mathbf{r}})\right|^2, \quad (9)$$

where k_z represents the longitudinal component of $\mathbf{k}_c$.

For the transverse momentum distribution in cylindrical coordinates $k_\perp \equiv \mathbf{k}_c^\perp = \sqrt{k_x^2+k_y^2}$

$$\frac{d\sigma_{\rm str}}{d^2k_\perp} = \frac{1}{(2\pi)^2}\frac{1}{2l_b+1}\int_0^\infty d^2b_p\left[1-|S_p\left(b_p\right)|^2\right] \times \sum_{m_b}\int_{-\infty}^{\infty} dz \left|\int d^2\rho\; \exp\left(-i\mathbf{k}_c^\perp.\boldsymbol{\rho}\right) S_c\left(b_c\right) \times g^{A\lambda J_b}_{(l_b\frac{1}{2})j_b;A-1\alpha I_1}(r) Y_{l_b m_b}(\hat{\mathbf{r}})\right|^2. \quad (10)$$

It is also convenient to describe the transverse momentum distributions in terms of the projection onto one of the Cartesian components of the transverse momentum, i.e.

$$\frac{d\sigma_{\rm str}}{dk_y} = \int dk_x \; \frac{d\sigma_{\rm str}}{d^2k_\perp}\left(k_x, k_y\right) \; . \tag{11}$$

The total stripping cross section can be obtained by integrating either Eq. (9) or Eq. (10). The integrals in Eqs. (9), (10), and for the total cross sections, are done numerically with use of Gaussian expansions of the S-matrices, as explained in Ref. [40].

The S-matrices have been obtained using the optical limit of the Glauber theory, i.e.

$$S_i\left(b\right) = \exp\left[\frac{i}{k_{NN}}\int_0^\infty dq \; q\rho_i\left(q\right)\rho_t\left(q\right)f_{NN}\left(q\right)J_0\left(qb\right)\right], \tag{12}$$

where $\rho_{i,t}\left(q\right)$ is the Fourier transform of the nuclear densities of the incident particle (i = p, ^{7}Be) and target (t), and $f_{NN}\left(q\right)$ is the high-energy nucleon-nucleon scattering amplitude at forward angles, which can be parametrized by [41]

$$f_{NN}\left(q\right) = \frac{k_{NN}}{4\pi}\sigma_{NN}\left(i+\alpha_{NN}\right)\exp\left(-\beta_{NN}q^2\right) \; . \tag{13}$$

In this equation σ_{NN}, α_{NN}, and β_{NN} are parameters which fit the high-energy nucleon-nucleon scattering at forward angles [41]. We use the values from Ref. [42] which have been extended to collisions at lower energies and corrected for isospin-average. The quantities $\rho_i\left(q\right)$ (i = p, ^{7}Be) and $\rho_t\left(q\right)$ are calculated from radial density distributions taken to be of Gaussian shapes, adjusted to reproduce the rms radius of the proton, ^{7}Be, ^{9}Be and ^{12}C, respectively.

The Coulomb part of the eikonal phase is included according the prescription described in details in Ref. [40].

As seen from Eqs. (9) and (10), the longitudinal and transverse momentum distributions, as described above, is a direct test of the ^{8}B ground state wave function calculated with the NCSM. We do this by comparing to two sets of experimental data. First we compare to an experiment performed at MSU for the transverse momentum distributions of ^{7}Be fragments from the reaction ^{8}B+^{9}Be at 41 MeV/nucleon [43]. In spite of the absence of gamma-ray coincidence data, this is a favorable case because the ground-state cross section dominates and because the approximately 15% branch to the excited level also has l=1 and has an almost identical shape. Because the data is given in arbitrary units, we have multiplied the contributions for the momentum distributions from each angular momentum channel by the same factor so that their sum reproduces the maximum of the experimental distribution. Thus, by comparing our results to this experiment we are testing the relative ratios between the ^{8}B spectroscopic factors obtained with the NCSM. Figures 14 and 15 shows our calculations with the CD-Bonn and INOY interactions, respectively. The WS solution fit procedure was employed to correct the asymptotics of the NCSM overlap functions. We used the $10\hbar\Omega$ model space and the optimal HO frequencies of $\hbar\Omega = 12$ MeV and $\hbar\Omega = 16$ MeV as determined from the ground-state-energy dependencies for the CD-Bonn and INOY potentials, respectively. In both cases one notices that our calculations are in excellent agreement with the data, which they reproduce over two orders of magnitude in cross section.

From Figs. 14 and 15 it is difficult to judge the quality of the CD-Bonn and the INOY interaction in reproducing the momentum distributions. Except from a noticeable visual difference seen for the magnitude of individual contributions for the 3 distinct ^{8}B states, the shape of the total distributions is essentially the same for the two interactions.

We perform another comparison, this time for the longitudinal momentum distributions, using Eq. (9). The data are taken from a GSI experiment [44] which measured gamma rays in coincidence with ^{7}Be residues and separated the cross sections to the three final states in the reaction ^{8}B +^{12} C at 936 MeV/nucleon. Figure 16 shows the data, which are in reasonably good agreement with calculations. The full drawn curves represent theoretical calculations using the NCSM with the CD-Bonn 2000 interaction. The sum of the three theoretical contributions is shown by a dashed-line. The experimental cross section is $\sigma_{-p} = 94 \pm 9$ mb, whereas the theoretical one, with NCSM wave functions and the CD-Bonn 2000 interaction, is 99.66 mb, in excellent agreement with the experimental one. The theoretical total momentum distribution for this reaction is wider than the experimental data. The experimental FWHM (full width at half maximum) is 95 ± 5 MeV/c if fitted by a single Gaussian. The theoretical one has a longer tail than the experimental one. It can be fitted by two Gaussians. The width of the narrower Gaussian is 96 MeV/c, also in good agreement with the experimental data. The reason for the longer tail in the theoretical momentum distribution is not well known, although a possible explanation is that the comparison between experiment and theory, as described in Ref. [44], involves a folding with the experimental resolution and a scaling to match the amplitude of the experimental spectrum, which has not been done here.

Figure 17 shows our results for exclusive p_z distribution, considering only the core excited contribution. The solid curve is the calculation using NCSM wave function with the CD-Bonn 2000 interaction. The data, from Ref. [44], has a width of 109 ± 7 MeV/c and the theoretical one is 112 MeV/c. The total experimental cross section for the excitation of this state is $\sigma_{-p} = 12 \pm 3$ mb, whereas the theoretical one is 16.36 mb, again in good agreement with the data.

Figures 18 and 19 are the same as the respective Figs. 16 and 17, but for NCSM wave functions calculated with the INOY interaction. The theoretical cross section for the inclusive reaction is 82.93 mb, and 13.17 mb for the inclusive cross section for the excited state. These

cross sections are smaller than the ones obtained with the CD-Bonn 2000 interaction. The probable reason is that the INOY interaction yields a smaller $\langle r^2\rangle_{\rm rms}$-value than the CD-Bonn 2000 interaction. The calculations yield 92 MeV/c and 108 MeV/c for the for the inclusive and the excited state momentum distribution widths, respectively. Table VII summarizes the calculations for the total cross sections.

V. S-FACTOR FOR ^{7}Be(p,γ)^{8}B

We now turn our focus to the S-factor for the reaction ^{7}Be(p,γ)^{8}B. This reaction is very important to understand the structure of our sun. The high energy neutrinos from the beta-decay of ^{8}B come from the sun's center and, therefore, are a direct measure of the conditions in its interior (temperature, pressure, chemical composition, etc.). The wave functions calculated with NCSM method, described in the previous sections will be used for the purpose.

The main contribution to the S-factor for the radiative capture reaction ^{7}Be(p,γ)^{8}B is due to the electric dipole multipolarity [37]. To calculate the S-factor, we have to evaluate a matrix element of the E1 operator $E1 = \sum_{i=1}^{A} e_i(\vec{r}_i - \vec{R})$ with $e_i = e$ for a proton and $e_i = 0$ for a neutron and the center of mass coordinate $\vec{R} = \frac{1}{A}\sum_i \vec{r}_i$. Using the notation introduced in Eqs. (1) and (2), we calculate a transition from a continuum state $|\mathcal{A}\Phi^{(A-1,1)J_c}_{(l_c\frac{1}{2})j_c;\alpha I_1};\delta_r\rangle\varphi^E_{l_cj_c\alpha I_1J_c}(r)$ to the bound state $|A\lambda J_b\rangle$. Here, $\varphi^E_{l_cj_c\alpha I_1J_c}(r)$ is the scattering wave function of the ^{7}Be+p relative motion. As the internal excitation of ^{7}Be by the E1 operator will have a negligible overlap with the ^{8}B ground state, we arrive at the following result

$$
\begin{aligned}
&\int_0^\infty dr r^2\langle A\lambda J_b||E1^{(1)}||\mathcal{A}\Phi^{(A-1,1)J_c}_{(l_c\frac{1}{2})j_c;\alpha I_1};\delta_r\rangle\varphi^E_{l_cj_c\alpha I_1J_c}(r)\\
&\approx \frac{Z_{A-1}-(A-1)}{A}e\sqrt{\frac{4\pi}{3}}\sqrt{A}\\
&\times\int_0^\infty dr r^2\langle A\lambda J_b||rY_1||\Phi^{(A-1,1)J_c}_{(l_c\frac{1}{2})j_c;\alpha I_1};\delta_r\rangle\varphi^E_{l_cj_c\alpha I_1J_c}(r)\\
&=\frac{Z_{A-1}-(A-1)}{A}e\sum_{l_bj_b}\left\{\begin{array}{ccc}1 & J_b & J_c\\ I_1 & j_c & j_b\end{array}\right\}\hat{J}_b\hat{J}_c\\
&\times\hat{j}_b\hat{j}_c(-1)^{j_b+j_c+I_1+J_c-\frac{1}{2}}\left(\begin{array}{ccc}j_c & 1 & j_b\\ -\frac{1}{2} & 0 & \frac{1}{2}\end{array}\right)\\
&\times\int_0^\infty dr g^{A\lambda J_b}_{(l_b\frac{1}{2})j_b;A-1\alpha I_1}(r)r^3\varphi^E_{l_cj_c\alpha I_1J_c}(r)\,, \qquad (14)
\end{aligned}
$$

with $|A\lambda J_b\rangle$ the ground state of ^{8}B with $J^\pi_b = 2^+$ and $|A-1\alpha I_1\rangle$ the ground state of ^{7}Be with $I^\pi_1 = \frac{3}{2}^-$. The ^{7}Be proton number Z_{A-1} is equal to 4. The overlap integral $g^{A\lambda J_b}_{(l_b\frac{1}{2})j_b;A-1\alpha I_1}(r)$ is defined as in Eq. (2) with its asymptotic tail corrected as described in Sect. III B. Assuming that the relative-motion scattering wave function is independent on the continuous state total angular momentum J_c, $\varphi^E_{l_cj_c\alpha I_1J_c}(r) = \varphi^E_{l_cj_c\alpha I_1}(r)$, we arrive at the S-factor expression [11, 37]

$$
\begin{aligned}
S(E) &= \frac{4\pi^2e^2_{\rm eff}\hbar^2}{3\mu_{\rm p^7Be}}\left(\frac{E+E_b}{\hbar c}\right)^3\exp\left[2\pi\eta(E)\right]\\
&\times\frac{(2J_b+1)}{2(2I_1+1)}\sum_{l_bj_bl_cj_c}\left(\begin{array}{ccc}j_c & 1 & j_b\\ -\frac{1}{2} & 0 & \frac{1}{2}\end{array}\right)^2\\
&\times\left|\int_0^\infty dr g^{A\lambda J_b}_{(l_b\frac{1}{2})j_b;A-1\alpha I_1}(r)r^3\varphi^E_{l_cj_c\alpha I_1}(r)\right|^2 , \qquad (15)
\end{aligned}
$$

where E_b is the binding energy of the ^{8}B bound state with respect to ^{7}Be+p. Further, $\eta(E) = Z_aZ_Ae^2/\hbar v_{\rm p^7Be}$ is the Sommerfeld parameter, k is the relative momentum, $E = \hbar^2k/2\mu_{\rm p^7Be}$ is the center-of-mass energy of the proton+^{7}Be, and $e_{\rm eff} = \frac{(A-1)-Z_{A-1}}{A}e = 3e/8$ is the effective charge for the E1 capture for this specific reaction. The continuum wave functions are normalized so that

$$
\begin{aligned}
&r\varphi^E_{l_cj_c\alpha I_1}(r\to\infty)\longrightarrow\\
&i\sqrt{\frac{\mu_{\rm p^7Be}}{2\pi k\hbar^2}}\left[H^{(-)}_{l_c}(r)-\mathcal{S}_{l_cj_c}H^{(+)}_{l_c}(r)\right]e^{i\sigma_{l_c}(E)}, \qquad (16)
\end{aligned}
$$

where $\mathcal{S}_{l_cj_c} = \exp\left[2i\delta_{l_cj_c}\right]$, with $\delta_{l_cj_c}$ (σ_{l_c}) being the nuclear (Coulomb) phase shift, and $H^{(\pm)}_{l_c}(r) = G_{l_c}(r) \pm iF_{l_c}(r)$, with F_{l_c} and G_{l_c} being the regular and irregular Coulomb wave functions, respectively. The normalization (16) implies that the continuum wavefunctions satisfy the relation

$$
\left\langle\varphi^E_\eta|\varphi^{E'}_{\eta'}\right\rangle = \delta\left(E-E'\right)\delta_{\eta\eta'}.
$$

Eq. (15) shows that the S-factor is a more stringent test of the nuclear model. Whereas the momentum distributions discussed in the previous section depends only on the bound state overlap function, $g^{A\lambda J_b}_{(l_b\frac{1}{2})j_b;A-1\alpha I_1}(r)$, obtained from the corrected NCSM overlap integrals discussed in subsection III B, the S-factor also depends on the continuum wave function, $\varphi^E_{l_cj_c\alpha I_1}(r)$. Presently, we have not yet developed a theory to extend the NCSM in order to describe continuum wave functions. Therefore, to obtain $\varphi^E_{l_cj_c\alpha I_1}(r)$ for s and d waves, we use a potential model with a Woods-Saxon+Coulomb+spin-orbit interaction. In this respect, our approach is similar to that by Nollett *et al.* [45, 46] where *ab initio* variational Monte Carlo wave functions were used in combination with cluster-cluster potential model scattering wave functions to describe d(α,γ)^{6}Li, ^{3}H(α,γ)^{7}Li and ^{3}He(α,γ)^{7}Be capture reactions. Since the largest part of the integrand of the last term in Eq. 15 stays outside the nuclear interior, one expects that the continuum wave functions are well described by this model. It is possible to use for this purpose the same WS potential that we obtained from correcting the bound-state overlap integral. Then we would have a different scattering state for each bound-state partial wave and each NCSM model space

and HO frequency. In order to have the same scattering wave function in all the calculations, we chose a WS potential from Ref. [38] that was fitted to reproduce the p-wave 1^+ resonance in ^{8}B. It was argued [11] that such a potential is also suitable for the description of s- and d-waves. The parameters of this potential are summarized in Table VI.

We note that the S-factor results are very weakly dependent on the choice of the potential that describes the scattering state. This is in particular true at low energies. Using our fitted potentials for the scattering state instead of the scattering potential from Table VI changes (typically increases) the S-factor by less than 1.5 eV b at 1.6 MeV with still a smaller change at lower energies and no change at 0 MeV.

At the same time, we note that the ^{7}Be+p scattering length has been measured [47]. A potential model with no spin-orbit term was developed in Ref. [13] that fits the experimental scattering length. It is not consistent to use that potential in the present work, as we employ an alternative angular momentum coupling scheme. Still, to get a further insight on the S-factor energy dependence sensitivity to the scattering wave function, we performed test calculations with the $s = 2$ potential of Ref. [13]. Up to 100 keV, we observed very little change of the S-factor compared to the situation when the scattering potential from Table VI was used. At higher energies, the S-factor increased by up to 5 eV b with a difference of 4 eV b at 1.6 MeV. To resolve the issue of the S-factor energy dependence at higher energies, we need to develop a theory that extends the NCSM to describe scattering states. This is a subject of current and future investigations.

In Fig. 20, we present our first application for the astrophysical S-factor of the $^7\mathrm{Be}(\mathrm{p},\gamma)^8\mathrm{B}$ reaction. We use bound-state wave functions calculated with the CD-Bonn 2000 interaction in the $10\hbar\Omega$ model space and the optimal HO frequency $\hbar\Omega = 12$ MeV. The WS solution fit procedure was employed to correct the asymptotics of the NCSM overlap functions. In the figure, we show the S-factor contributions from the dominant $l = 1$, $j = 3/2$ and $j = 1/2$ partial waves by the dashed lines. Clearly, the $j = 3/2$ partial wave is the most important one. The upper curve, the full line, is the sum of the two contributions. The experimental data is a compilation of the latest experiments for the S-factor. They include direct, as well as some indirect measurements (Coulomb dissociation).

The slope of the curve corresponding to the total S-factor follows the trend of the data. From Fig. 20 it is also clear that the spectroscopic factors for the $l = 1$, $j = 3/2$ and $j = 1/2$ partial waves are well described within the NCSM and the CD-Bonn 2000 interaction. Our calculation presented in Fig. 20 is in a very good agreement with the recent direct measurement data of Ref. [7]. We note that our S-factor energy dependence more resembles that obtained within the three-cluster model of Ref. [16] rather than that obtained within the potential model of Ref. [13].

In order to judge the convergence of our S-factor calculation, we performed a detailed investigation of the model-space-size and the HO frequency dependencies. The dependence of the $^7\mathrm{Be}(\mathrm{p},\gamma)^8\mathrm{B}$ S-factor on the size of the basis from $6\hbar\Omega$ to $10\hbar\Omega$ corresponding to the above discussed calculation using the CD-Bonn 2000 and the HO frequency of $\hbar\Omega = 12$ MeV is shown in Fig. 21. One observes a very little model-space dependence with some oscillatory behavior. The fact that the calculation converges for a basis size within this energy interval demonstrates that the optimal HO frequency determined from the ground-state energy calculation is also close to optimal for the S-factor calculation.

To further investigate the HO frequency sensitivity, we show in Fig. 22 the dependence of the $^7\mathrm{Be}(\mathrm{p},\gamma)^8\mathrm{B}$ S-factor on the HO frequency from $\hbar\Omega = 11$ MeV to $\hbar\Omega = 15$ MeV. The CD-Bonn 2000 NN potential and the $10\hbar\Omega$ model space were used. Again, the WS solution fit procedure was employed to correct the asymptotics of the NCSM overlap functions. In all cases, we obtain basically identical energy dependence. The absolute values of the S-factor increase with decreasing frequency. To determine the optimal frequency and interpolate the converged S-factor result, we examine the basis size dependence for different HO frequencies. In Fig. 23, we show the $\hbar\Omega = 15$ MeV results for model spaces from $6\hbar\Omega$ to $10\hbar\Omega$. We observe a steady increase of the S-factor with the basis size enlargement. Contrary to this situation, the calculation using the HO frequency of $\hbar\Omega = 11$ MeV presented in Fig. 24 shows that the S-factor does not increase any more with increasing $N_{\max}$. Actually, there is a small decrease when going from the $8\hbar\Omega$ to the $10\hbar\Omega$. In Table VIII, we summarize our S-factors at 10 keV obtained for different frequencies and model spaces. In addition to the results obtained using the WS solution fit procedure, we also present the S_{17} and the ANC obtained using the alternative direct Whittaker matching procedure. We note that the ANC from our *ab initio* approach are smaller than those obtained within the microscopic three-cluster model [16] but still larger than the experimental ones from the DWBA analysis of Ref. [48]. In general, both procedures lead to basically identical energy dependence with a difference of about 1 to 2 eV b in the S-factor with the smaller values from the direct Whittaker function matching procedure. Taking into account that in the case of the direct Whittaker function matching the S_{17} increases with $N_{\max}$ even at the HO frequency of $\hbar\Omega = 11$ MeV, unlike in the case of the WS solution fit procedure, results of the two approaches do not contradict each other. Combining all these results, we determine that the optimal frequency is between $\hbar\Omega = 11$ and 12 MeV. Results in this frequency region show very weak dependence on $N_{\max}$, with relative difference between the two methods always in the range of 5 to 8%. The full range of results is covered by $S_{17}(10\ \mathrm{keV}) = 22.1 \pm 1.0$ eV b.

We have performed a similar, although a less extensive study for the INOY NN interaction. In Fig. 25, we

present the S-factor and its partial wave contributions as obtained using the INOY NN interaction and the ground-state-energy-determined optimal frequency of $\hbar\Omega = 16$ MeV. The $10\hbar\Omega$ model space and the WS solution fit procedure was utilized. The energy dependence is slightly weaker compared to the CD-Bonn case and the S-factor underestimates most of the experimental data. To make a direct comparison with the CD-Bonn calculation, in Fig. 26 we show S-factors obtained from the CD-Bonn 2000 and the INOY NN potentials using identical HO frequency of $\hbar\Omega = 14$ MeV and the $10\hbar\Omega$ model space. Although the spectroscopic factors are almost the same, see Table V, the INOY S-factor is significantly smaller than that of the CD-Bonn 2000. This is a consequence of different shapes of the overlap functions displayed in Fig. 13. This result is correlated with our radius and quadrupole moment results as well as results of momentum distributions in knockout reactions. The fact that the INOY NN interaction yields a smaller matter radii than the CD-Bonn 2000 leads to a smaller S-factor. The S-factor convergence for the INOY NN potential is similar or better than for the CD-Bonn 2000. Based on the results presented in the figures and the Table VIII, we estimate the INOY S-factor result at 10 keV to be 19.0 ± 1 eV b.

VI. CONCLUSIONS

We studied nuclear structure of ^{7}Be, ^{8}B and ^{7,8}Li within the *ab initio* NCSM. We calculated overlap integrals of the ^{8}B ground state with ^{7}Be+p as a function of the separation between the proton and ^{7}Be using NCSM wave functions obtained in model spaces up to $10\hbar\Omega$. Assuming that the NCSM overlap integrals are realistic in the interior part, we utilized Woods-Saxon potential as a tool to correct their asymptotics. We performed a least-square fit of WS potential solutions to the NCSM overlap integrals in the range from 0 fm up to about 4 fm under the constraint that the experimental separation energy is reproduced. In addition, we employed an alternative procedure of a direct Whittaker function matching to correct the asymptotic tail of the NCSM overlap integrals. The corrected overlap integrals were then used for the ^{7}Be(p,γ)^{8}B S-factor calculation. We investigated the dependence of the S-factor on the size of the model space and on the HO frequency as well as on the procedure of the asymptotic tail correction. Based on this investigation, we arrived at the S-factor result at 10 keV to be 22.1 ± 1.0 eV b and 19.0 ± 1.0 eV b for the CD-Bonn 2000 and INOY NN potentials, respectively. We note that the CD-Bonn 2000 results for the point-proton rms radii, quadrupole moments and momentum distributions in knockout reactions with ^{8}B projectiles are in a better agreement with experiment than those obtained using the INOY NN potential. At the same time, the CD-Bonn 2000 predicts the point-proton rms radii of ^{4}He and ^{6}He in agreement with experiment, while the INOY NN potential underpredicts both [49]. Therefore, we consider the CD-Bonn 2000 S-factor result more realistic. The energy dependence as well as the zero energy value of the S-factor calculated using the CD-Bonn 2000 NN potential are in a very good agreement with recent direct measurement data of Ref. [7]. We stress that no adjustable parameters were used in our *ab initio* calculations of the ^{8}B and ^{7}Be bound states. Taking into account that the S-factor is only weakly dependent on the potential model used to obtain the scattering state, we consider our results as the first *ab initio* prediction of the ^{7}Be(p,γ)^{8}B S-factor, in particular of its normalization.

Acknowledgments

We thank W. E. Ormand, C. Forssén and J. Dobeš for useful discussions. This work was partly performed under the auspices of the U. S. Department of Energy by the University of California, Lawrence Livermore National Laboratory under contract No. W-7405-Eng-48. Support from the LDRD contract No. 04–ERD–058, and from U.S. Department of Energy, Office of Science, (Work Proposal Number SCW0498), and grant No. DE-FG02-04ER41338, is acknowledged.

[1] E. Adelberger *et al.*, Rev. Mod. Phys. **70**, 1265 (1998).
[2] SNO Collaboration, S. N. Ahmed *et al.*, Phys. Rev. Lett. **92**, 181301 (2004).
[3] S. Couvidat, S. Turck-Chièze, and A. G. Kosovichev, Astrophys. J. **599**, 1434 (2003).
[4] J. N. Bahcall and M. H. Pinsonneault, Phys. Rev. Lett. **92**, 121301 (2004).
[5] B. W. Filippone, A. J. Elwyn, C. N. Davids, and D. D. Koetke, Phys. Rev. Lett **50**, 412 (1983); Phys. Rev. C **28**, 2222 (1983).
[6] L.T. Baby *et al.*, Phys. Rev. Lett. **90**, 022501 (2003).
[7] A. R. Junghans, E. C. Mohrmann, K. A. Snover, T. D. Steiger, E. G. Adelberger, J. M. Casandjian, H. E. Swanson, L. Buchmann, S. H. Park, A. Zyuzin, and A. M. Laird, Phys. Rev. C **68**, 065803 (2003).
[8] G. Baur, C.A. Bertulani and H. Rebel, Nucl. Phys. **A458**, 188 (1986).
[9] N. Iwasa *et al.*, Phys. Rev. Lett. **83**, 2910 (1999); B. Davids *et al.*, Phys. Rev. Lett. **86**, 2750 (2001); F. Schumann *et al.*, Phys. Rev. Lett. **90**, 232501 (2003).
[10] F. C. Barker, Nucl. Phys. **A588**, 693 (1995).
[11] R. G. H. Robertson, Phys. Rev. C **7**, 543 (1973).
[12] S. Typel, H. H. Wolter, and G. Baur, Nucl. Phys. **A613**, 147 (1997).
[13] B. Davids and S. Typel, Phys. Rev. C **68**, 045802 (2003).
[14] P. Descouvemont and D. Baye, Nucl. Phys. **A567**, 341

(1994).
[15] A. Csótó, K. Langanke, S. E. Koonin, and T. D. Shoppa, Phys. Rev. C **52**, 1130 (1995).
[16] P. Descouvemont, Phys. Rev. C **70**, 065802 (2004).
[17] P. Navrátil, J. P. Vary and B. R. Barrett, Phys. Rev. Lett. **84**, 5728 (2000); Phys. Rev. C **62**, 054311 (2000).
[18] P. Navrátil, G. P. Kamuntavičius and B. R. Barrett, Phys. Rev. C **61**, 044001 (2000).
[19] P. Navrátil and W. E. Ormand, Phys. Rev. C **68**, 034305 (2003).
[20] K. Suzuki and S. Y. Lee, Prog. Theor. Phys. **64**, 2091 (1980).
[21] K. Suzuki and R. Okamoto, Prog. Theor. Phys. **92**, 1045 (1994).
[22] E. Caurier, G. Martinez-Pinedo, F. Nowacki, A. Poves, J. Retamosa and A. P. Zuker, Phys. Rev. C **59**, 2033 (1999).
[23] E. Caurier and F. Nowacki, Acta Physica Polonica B **30**, 705 (1999).
[24] E. Caurier, P. Navrátil, W. E. Ormand and J. P. Vary, Phys. Rev. C **64**, 051301 (2001).
[25] E. Caurier, P. Navrátil, W. E. Ormand and J. P. Vary, Phys. Rev. C **66**, 024314 (2002).
[26] P. Navrátil, Phys. Rev. C **70**, 054324 (2004).
[27] R. Machleidt, Phys. Rev. C **63**, 024001 (2001).
[28] P. Doleschall, I. Borbély, Z. Papp, and W. Plessas, Phys. Rev. C **67**, 0064005 (2003).
[29] P. Doleschall, Phys. Rev. C **69**, 054001 (2004).
[30] R. Machleidt, F. Sammarruca and Y. Song, Phys. Rev. C **53**, 1483 (1996).
[31] D. R. Tilley, C. M. Cheves, J. L. Goodwin, G. M. Hale, H. M. Hofmann, J. H. Kelley, C. G. Sheu and H.R. Weller, Nucl. Phys. **A 708**, 3 (2002).
[32] J. H. Kelley, J. L. Goodwin, X. Hu, J. Purcell, C. G. Sheu, D. R. Tilley and H.R. Weller, Nucl. Phys. **A 745**, 155 (2004).
[33] S. C. Pieper, R. B. Wiringa, and J. Carlson, Phys. Rev. C **70**, 054325 (2004).
[34] R. D. Macfarlane and J. B. French, Rev. Mod. Phys. **32**, 567 (1960).
[35] J. P. Schiffer, G. C. Morrison, R. H. Siemssen, and B. Zeidman, Phys. Rev. **164**, 1274 (1967).
[36] S. Cohen and D. Kurath, Nucl. Phys. **A101**, 1 (1967).
[37] C. Bertulani, Comp. Phys. Comm. **156**, 123 (2003).
[38] H. Esbensen and G. F. Bertsch, Nucl. Phys. **A 600**, 37 (1996).
[39] M. Hussein and K. W. McVoy, Nucl. Phys. **A 445**, 124 (1985).
[40] C. A. Bertulani and P. G. Hansen, Phys. Rev. C **70**, 034609 (2004).
[41] L. Ray, Phys. Rev. C **20**, 1957 (1979).
[42] M. S. Hussein, R. Rego and C. A. Bertulani, Phys. Reports **201**, 279 (1991).
[43] J. H. Kelley *et al.*, Phys. Rev. Lett. **77**, 5020 (1967).
[44] D. Cortina-Gil *et al.*, Phys. Lett. **B 529**, 36 (2002).
[45] K. M. Nollett, R. B. Wiringa and R. Schiavilla, Phys. Rev. C **63**, 024003 (2001).
[46] K. M. Nollett, Phys. Rev. C **63**, 054002 (2001).
[47] C. Angulo *et al.*, Nucl. Phys. **A716**, 211 (2003).
[48] A. Azhari, V. Burjan, F. Carstoiu, C. A. Gagliardi, V. Kroha, A. M. Mukhamedzhanov, F. M. Nunes, X. Tang, L. Trache, and R. E. Tribble, Phys. Rev. C **37**, 2906 (1988).
[49] E. Caurier and P. Navrátil, nucl-th/0512015.

Figures

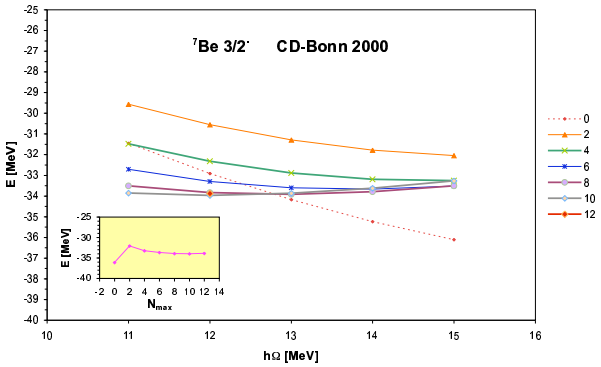

FIG. 1: HO frequency dependence of the ^{7}Be ground-state energy for model spaces from $0\hbar\Omega$ to $12\hbar\Omega$ obtained using the CD-Bonn 2000 NN potential. The inset demonstrates how the values at the minima of each curve converge with increasing $N_{\max}$.

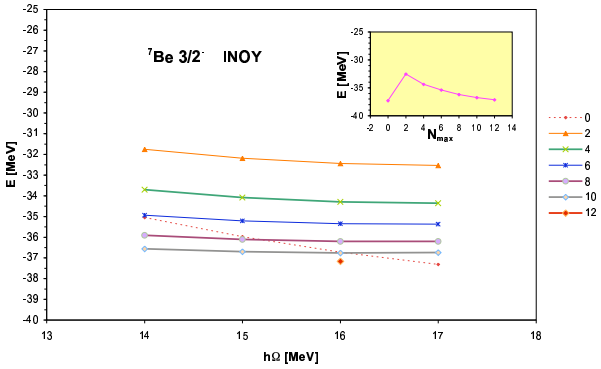

FIG. 2: Same as in Fig.1, but using the INOY NN potential.

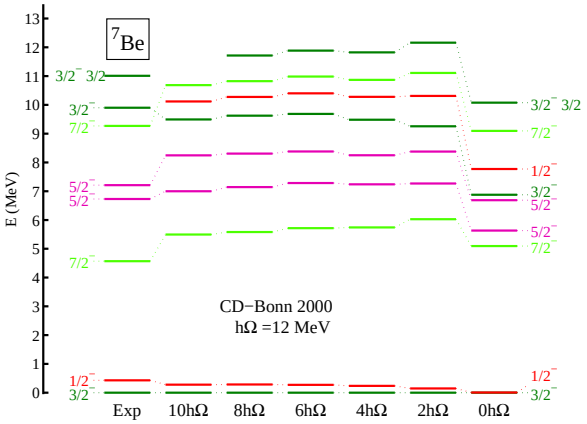

FIG. 3: Basis size dependence of the ^{7}Be excitation spectrum in the range from $0\hbar\Omega$ to $10\hbar\Omega$ obtained using the CD-Bonn 2000 NN potential and the HO frequency of $\hbar\Omega = 12$ MeV.

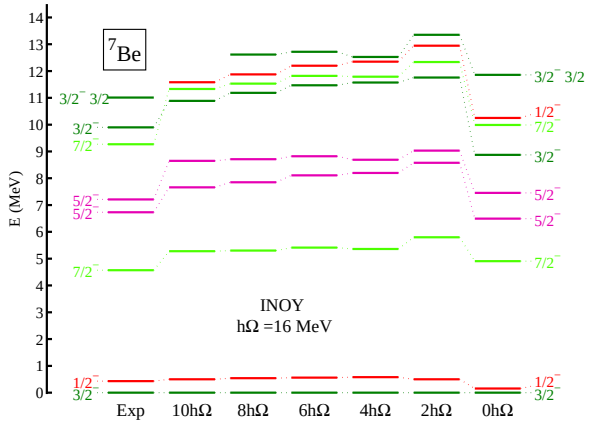

FIG. 4: Same as in Fig. 3, but using the INOY NN potential and the HO frequency of $\hbar\Omega = 16$ MeV.

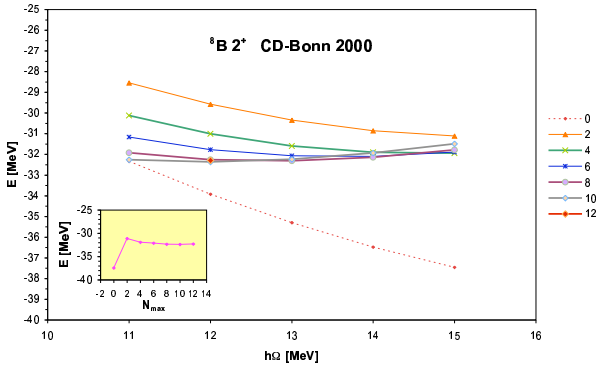

FIG. 5: HO frequency dependence of the ^{8}B ground-state energy for model spaces from $0\hbar\Omega$ to $12\hbar\Omega$ obtained using the CD-Bonn 2000 NN potential. The inset demonstrates how the values at the minima of each curve converge with increasing $N_{\max}$.

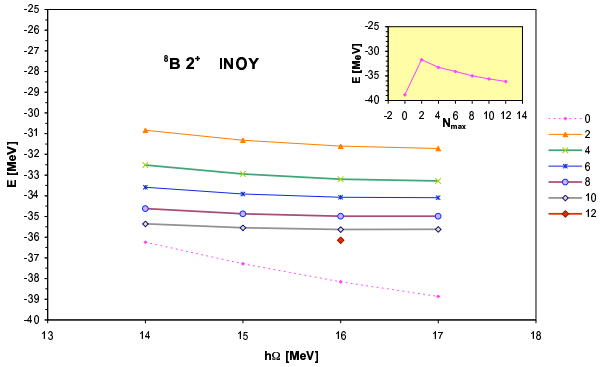

FIG. 6: Same as in Fig. 5, but using the INOY NN potential.

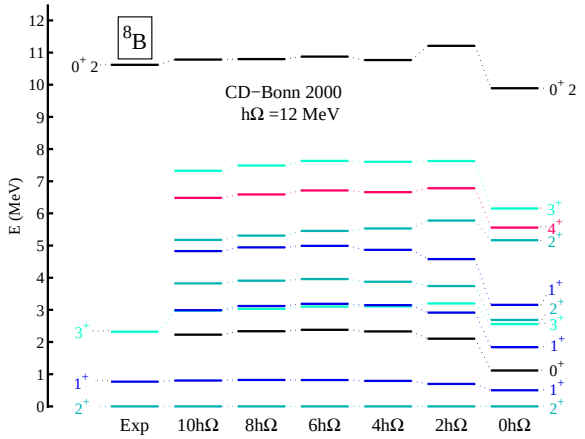

FIG. 7: Basis size dependence of the ^{8}B excitation spectrum in the range from $0\hbar\Omega$ to $10\hbar\Omega$ obtained using the CD-Bonn 2000 NN potential and the HO frequency of $\hbar\Omega = 12$ MeV.

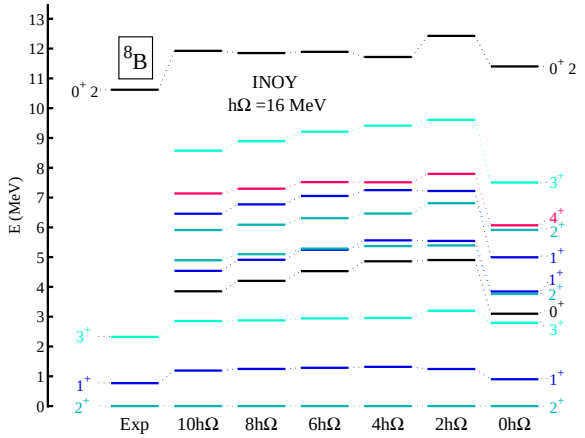

FIG. 8: Same as in Fig. 7, but using the INOY NN potential and the HO frequency of $\hbar\Omega = 16$ MeV.

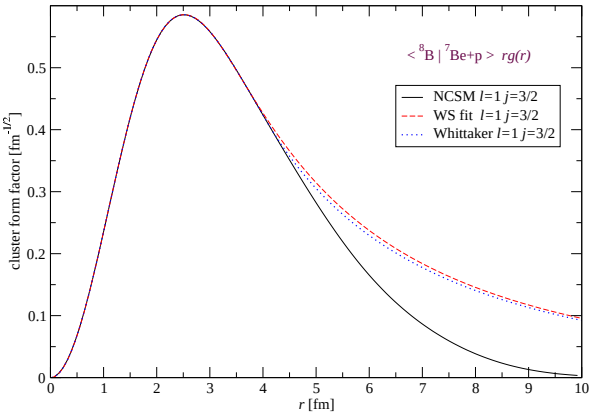

FIG. 9: Overlap integral, $rg(r)$, for the ground state of ^{8}B with the ground state of ^{7}Be plus proton as a function of separation between the ^{7}Be and the proton. The p-wave channel with $j = 3/2$ is shown. The full line represents the NCSM result obtained using the CD-Bonn NN potential in the $10\hbar\Omega$ model space and the HO frequency of $\hbar\Omega = 12$ MeV. The dashed line represents a corrected overlap obtained from a Woods-Saxon potential whose parameters were fit to the NCSM overlap up to 4.0 fm under the constraint to reproduce the experimental separation energy. The dotted line represents a corrected overlap obtained by a direct matching of the NCSM overlap and the Whittaker function.

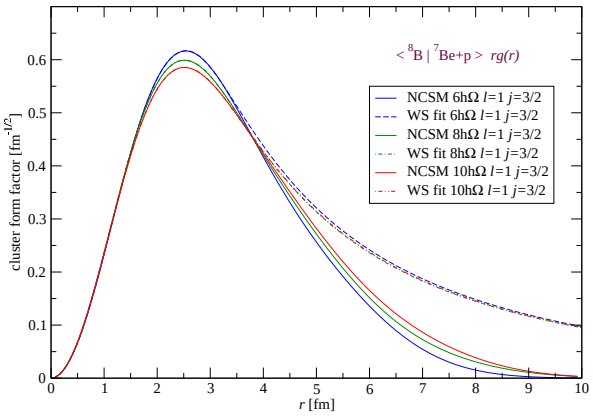

FIG. 10: Same as in Fig. 9, but for a comparison of results obtained using model spaces of $6, 8, 10\hbar\Omega$. Only corrections by the WS potential fit are shown. The fitting ranges up to 3.6, 3.8 and 4.0 fm were used, respectively.

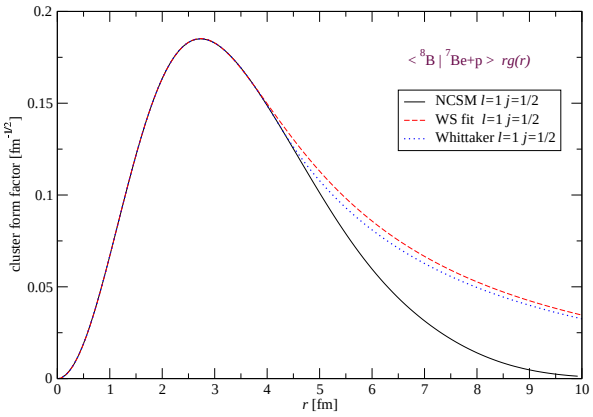

FIG. 11: Same as in Fig. 9, but for the p-wave channel with $j = 1/2$.

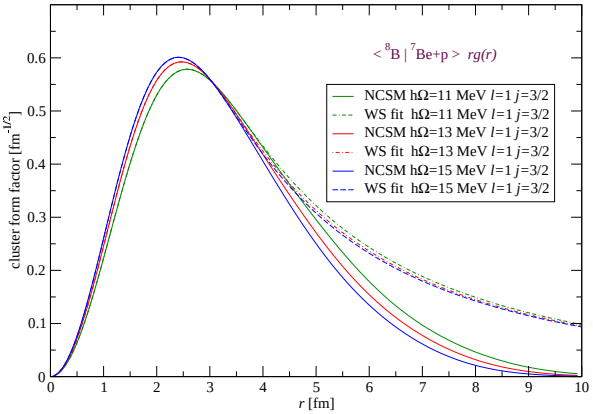

FIG. 12: Same as in Fig. 9, but for a comparison of results obtained using the HO frequencies of $\hbar\Omega = 11, 13, 15$ MeV. Only corrections by the WS potential fit are shown. The fitting ranges up to 4.0, 3.8 and 3.7 fm were used, respectively.

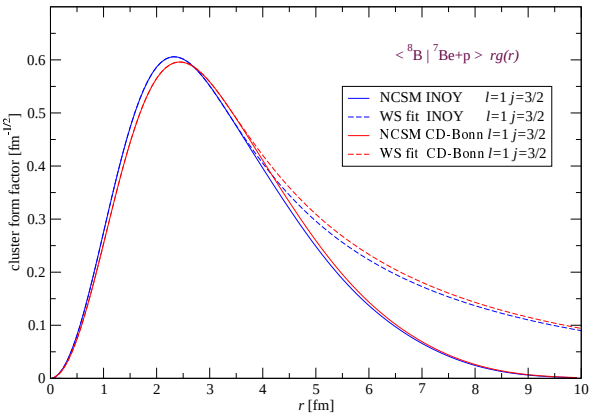

FIG. 13: Same as in Fig. 9, but using the HO frequency of $\hbar\Omega = 14$ MeV with results obtained by the CD-Bonn 2000 and INOY NN potentials shown for a comparison. Only corrections by the WS potential fit are shown. The fitting ranges up to 3.75 and 3.7 fm were used, respectively.

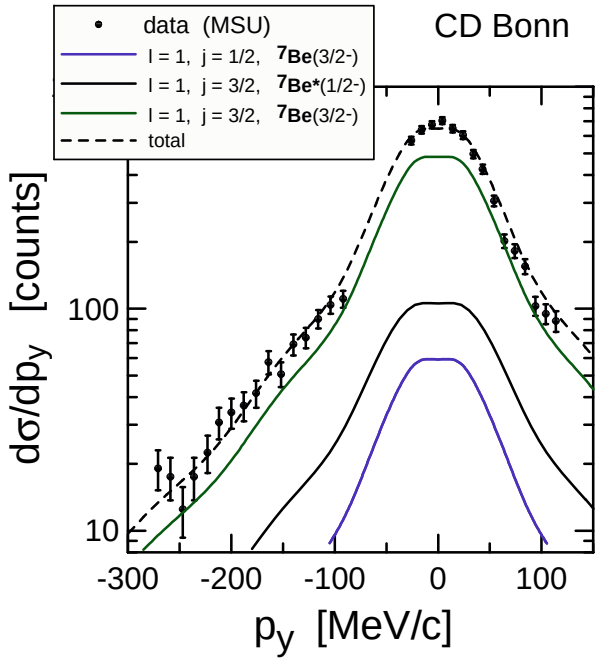

FIG. 14: Inclusive transverse-momentum distribution for the residue in the ^{9}Be(^{8}B,^{7}Be)X reaction measured at 41 MeV/nucleon [43]. The theoretical calculations are based on Eqs. 10 and 11 and using the CD-Bonn interaction for the ^{8}B NCSM wave function. The dotted curve is the sum of the individual contributions (full drawn). In order of increasing magnitude, the full curves correspond to $l = 1, j = 1/2$; ^{7}Be$(3/2^-)$, $l = 1, j = 3/2$; ^{7}Be$^*(1/2^-)$, and $l = 1, j = 3/2$; ^{7}Be$(3/2^-)$ states, respectively. The angular resolution in the experiment broadens the data by approximately 4%. This has not been included in the theoretical curves.

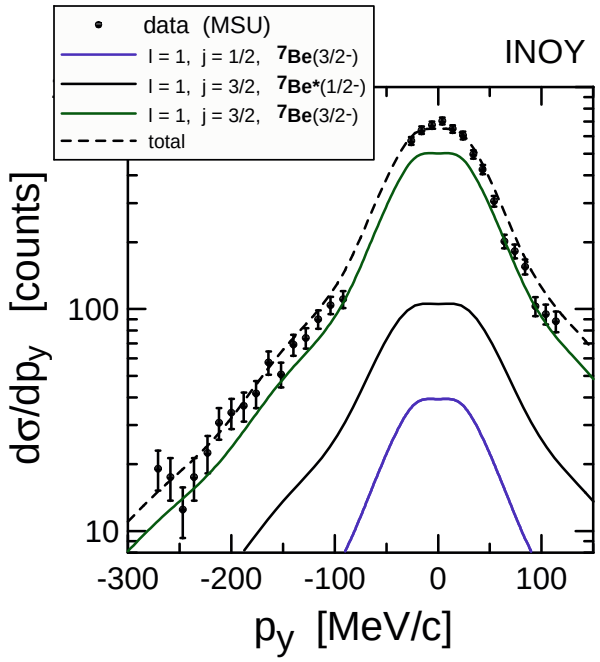

FIG. 15: Same as in Fig. 14, but using the INOY interaction for the ^{8}B NCSM wave function.

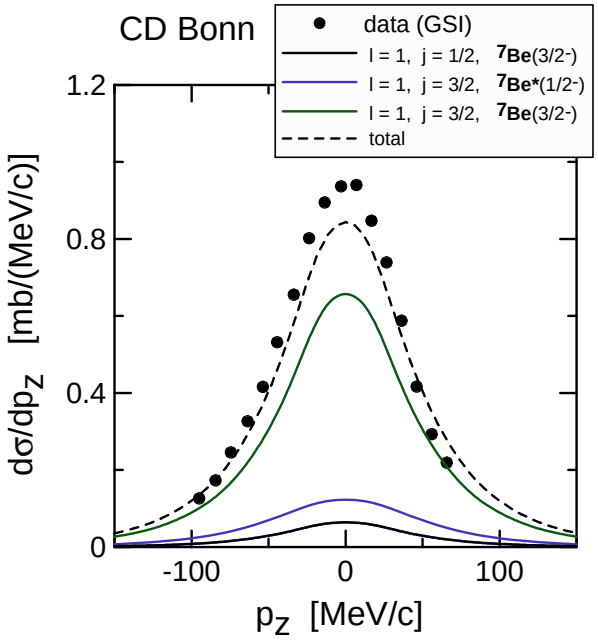

FIG. 16: Inclusive parallel momentum distribution of ^{7}Be fragments from the reaction ^{8}B+^{12}C$\longrightarrow^{7}$Be+X at 936 MeV/nucleon. The full drawn curves represent theoretical calculations using the NCSM with the CD-Bonn 2000 interaction. The sum of the three theoretical contributions is shown by a dashed-line.

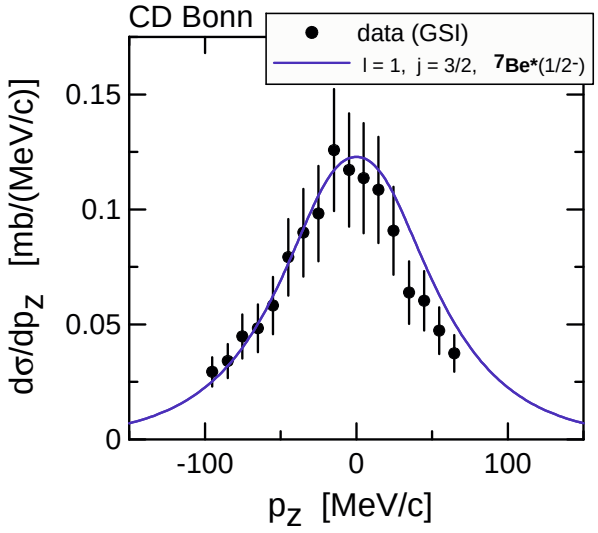

FIG. 17: Results for exclusive p_z distribution, considering only the core excited contribution. The solid curve is the calculation using NCSM wave function with CD-Bonn 2000 interaction.

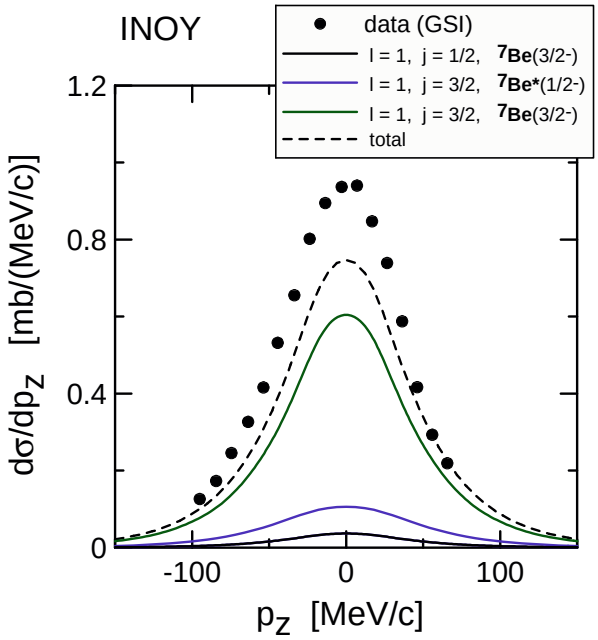

FIG. 18: Same as in Fig. 16, but using NCSM wave functions calculated with the INOY interaction.

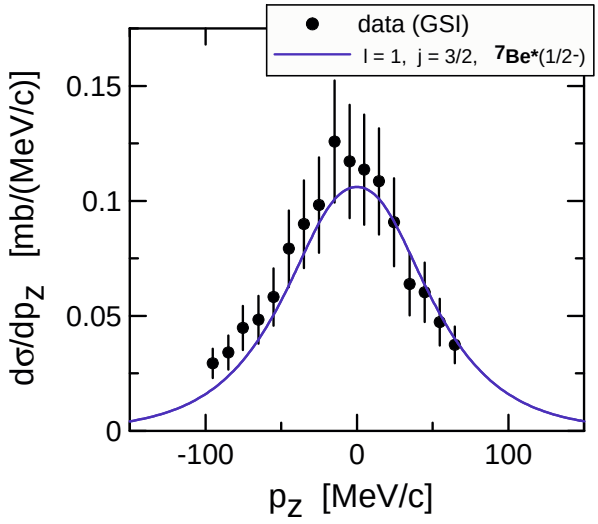

FIG. 19: Same as in Fig. 17, but using NCSM excited state wave function calculated with the INOY interaction.

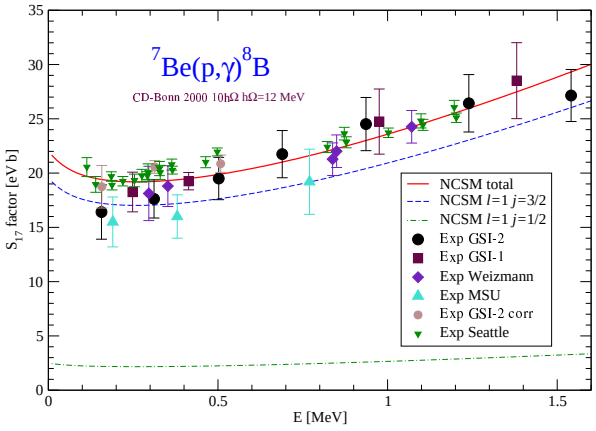

FIG. 20: The ^{7}Be(p,γ)^{8}B S-factor obtained using the NCSM cluster form factors with corrected asymptotics by the WS solution fit. The dashed and dashed-dotted lines show the contribution due to the $l = 1$, $j = 3/2$ and $j = 1/2$ partial waves, respectively. The CD-Bonn 2000 NN potential, the $10\hbar\Omega$ model space and the HO frequency of $\hbar\Omega = 12$ MeV were used. Experimental values are from Refs. [6, 7, 9].

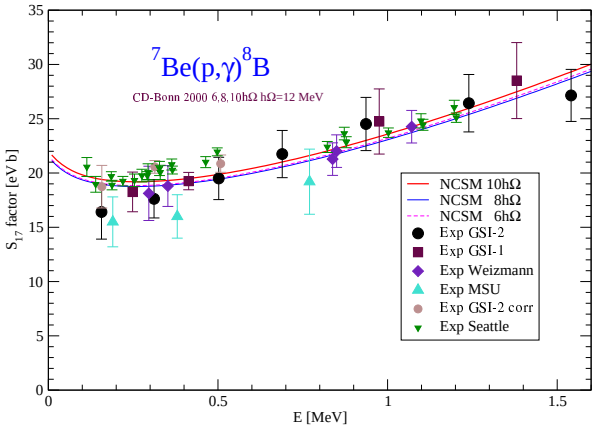

FIG. 21: The ^{7}Be(p,γ)^{8}B S-factor obtained using the NCSM cluster form factors with corrected asymptotics by the WS solution fit. The dependence on the size of the basis from $6\hbar\Omega$ to $10\hbar\Omega$ is shown. The CD-Bonn 2000 NN potential and the HO frequency of $\hbar\Omega = 12$ MeV were used. Experimental values are from Refs. [6, 7, 9].

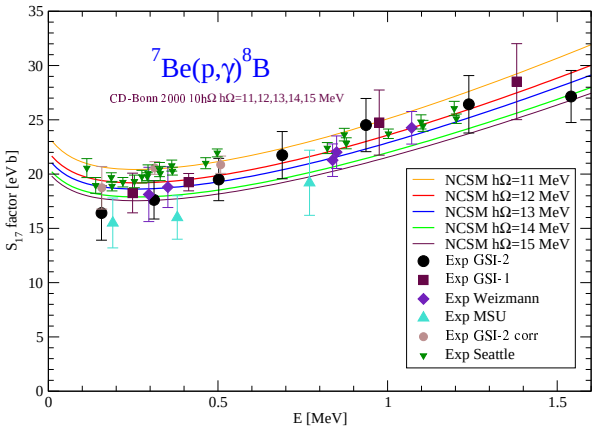

FIG. 22: The ^{7}Be(p,γ)^{8}B S-factor obtained using the NCSM cluster form factors with corrected asymptotics by the WS solution fit. The dependence on the size of the HO frequency from $\hbar\Omega = 11$ MeV to $\hbar\Omega = 15$ MeV is shown. The CD-Bonn 2000 NN potential and the $10\hbar\Omega$ model space were used. Experimental values are from Refs. [6, 7, 9].

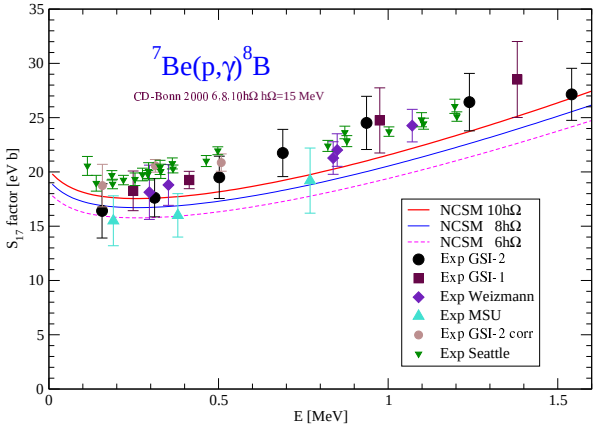

FIG. 23: Same as in Fig. 21 but for the HO frequency of $\hbar\Omega = 15$ MeV.

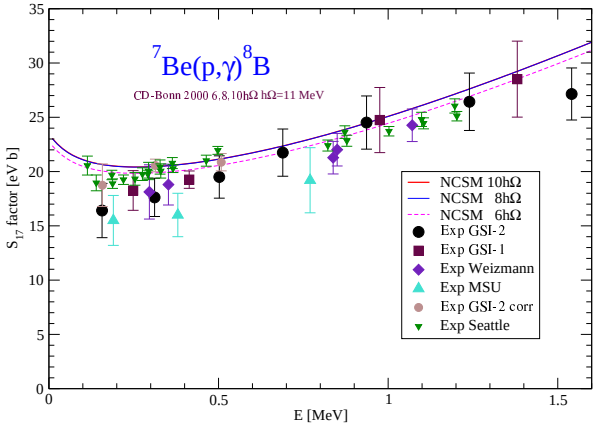

FIG. 24: Same as in Fig. 21 but for the HO frequency of $\hbar\Omega = 11$ MeV.

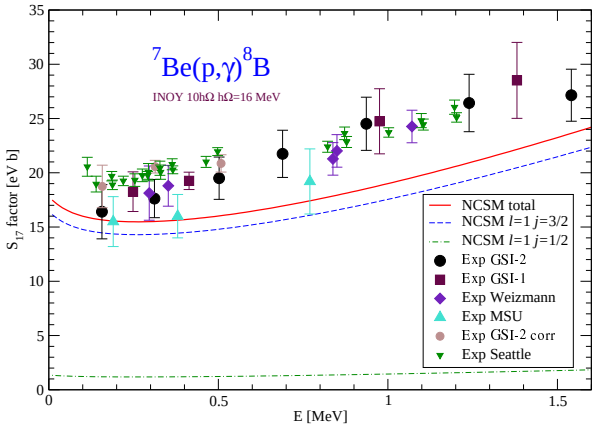

FIG. 25: Same as in Fig. 20 but for the INOY NN potential and the HO frequency of $\hbar\Omega = 16$ MeV.

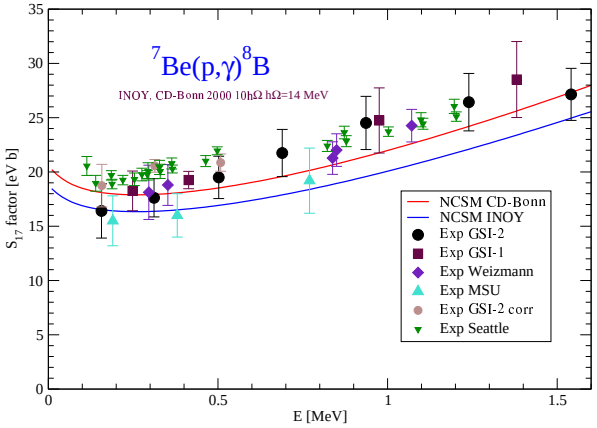

FIG. 26: The ^{7}Be(p,γ)^{8}B S-factor obtained using the NCSM cluster form factors with corrected asymptotics by the WS solution fit. The result obtained using the CD-Bonn and INOY NN potentials are compared. The $10\hbar\Omega$ model space and HO frequency of $\hbar\Omega = 14$ MeV were used. Experimental values are from Refs. [6, 7, 9].

Tables

TABLE I: The ^{7}Be and ^{7}Li ground and excited state energies (in MeV) obtained using the CD-Bonn 2000 and INOY NN potentials. The HO frequency of $\hbar\Omega = 12(16)$ MeV was used in the CD-Bonn 2000 (INOY) NN potential calculation. The ground (excited) state energies were obtained in the $12\hbar\Omega$ ($10\hbar\Omega$) model space. Experimental values are from Refs. [31].

	^{7}Be		
	Expt.	CD-Bonn 2000	INOY
$\lvert E_{\rm gs}(\frac{3}{2}^-_1\frac{1}{2})\rvert$	37.6004(5)	33.881	37.161
$E_{\rm x}(\frac{3}{2}^-_1\frac{1}{2})$	0.0	0.0	0.0
$E_{\rm x}(\frac{1}{2}^-_1\frac{1}{2})$	0.429	0.278	0.501
$E_{\rm x}(\frac{7}{2}^-_1\frac{1}{2})$	4.57(5)	5.494	5.278
$E_{\rm x}(\frac{5}{2}^-_1\frac{1}{2})$	6.73(10)	6.999	7.660
$E_{\rm x}(\frac{5}{2}^-_2\frac{1}{2})$	7.21(6)	8.247	8.648
$E_{\rm x}(\frac{7}{2}^-_2\frac{1}{2})$	9.27(10)	10.687	11.331
$E_{\rm x}(\frac{3}{2}^-_2\frac{1}{2})$	9.9	9.493	10.887
$E_{\rm x}(\frac{1}{2}^-_2\frac{1}{2})$		10.120	11.583
$E_{\rm x}(\frac{3}{2}^-_1\frac{3}{2})$	11.01(3)	11.717	12.607
	^{7}Li		
	Expt.	CD-Bonn 2000	INOY
$\lvert E_{\rm gs}(\frac{3}{2}^-_1\frac{1}{2})\rvert$	39.245	35.524	38.892
$E_{\rm x}(\frac{3}{2}^-_1\frac{1}{2})$	0.0	0.0	0.0
$E_{\rm x}(\frac{1}{2}^-_1\frac{1}{2})$	0.478	0.285	0.513
$E_{\rm x}(\frac{7}{2}^-_1\frac{1}{2})$	4.65	5.585	5.353
$E_{\rm x}(\frac{5}{2}^-_1\frac{1}{2})$	6.60	7.079	7.741

$E_x(\frac{5}{2}^-_2\frac{1}{2})$	7.45	8.522	8.902
$E_x(\frac{3}{2}^-_2\frac{1}{2})$	8.75	9.849	11.267
$E_x(\frac{1}{2}^-_2\frac{1}{2})$	9.09	10.458	11.931
$E_x(\frac{7}{2}^-_2\frac{1}{2})$	9.57	11.033	11.691
$E_x(\frac{3}{2}^-_1\frac{3}{2})$	11.24	11.974	12.826

TABLE II: The ^{7}Be and ^{7}Li point-proton rms radii (in fm), ground-state quadrupole (in $e$fm^2) and magnetic (in μ_N) moments and M1 transitions (in μ_N^2) obtained within the NCSM for different HO frequencies (given in MeV) and model spaces for the CD-Bonn 2000 and INOY NN potentials. Experimental values are from Refs. [31].

^{7}Be

CD-Bonn 2000

$\hbar\Omega$	$N_{\max}$	r_p	Q	μ	B(M1; $\frac{1}{2}^- \to \frac{3}{2}^-$)
12	6	2.311	-4.755	-1.150	3.192
12	8	2.324	-4.975	-1.151	3.145
12	10	2.342	-5.153	-1.141	3.114
12	12	2.365			
11	6	2.377	-5.029	-1.150	3.203
11	8	2.377	-5.186	-1.151	3.162
11	10	2.383	-5.354	-1.155	3.125
Expt.		2.36(2)		-1.398(15)	3.71(48)

INOY

$\hbar\Omega$	$N_{\max}$	r_p	Q	μ	B(M1; $\frac{1}{2}^- \to \frac{3}{2}^-$)
16	6	2.114	-3.946	-1.161	3.158
16	8	2.149	-4.212	-1.157	3.119
16	10	2.181	-4.459	-1.151	3.092
16	12	2.214			
14	6	2.190	-4.245	-1.162	3.180
14	8	2.209	-4.454	-1.158	3.139
14	10	2.227	-4.654	-1.155	3.108
Expt.		2.36(2)		-1.398(15)	3.71(48)

^{7}Li

CD-Bonn 2000

$\hbar\Omega$	$N_{\max}$	r_p	Q	μ	B(M1; $\frac{1}{2}^- \to \frac{3}{2}^-$)
12	6	2.149	-2.717	+3.027	4.256
12	8	2.156	-2.866	+3.020	4.188
12	10	2.168	-3.001	+3.011	4.132
12	12	2.188	-3.130		
Expt.		2.27(2)	-4.06(8)	+3.256	4.92(25)

INOY

$\hbar\Omega$	$N_{\max}$	r_p	Q	μ	B(M1; $\frac{1}{2}^- \to \frac{3}{2}^-$)
16	6	1.963	-2.334	+3.039	4.192
16	8	1.990	-2.500	+3.029	4.136
16	10	2.015	-2.648	+3.021	4.098
16	12	2.042	-2.788		
Expt.		2.27(2)	-4.06(8)	+3.256	4.92(25)

TABLE III: The ^{8}B and ^{8}Li ground and excited state energies (in MeV) obtained using the CD-Bonn 2000 and INOY NN potentials. The HO frequency of $\hbar\Omega = 12(16)$ MeV was used in the CD-Bonn 2000 (INOY) NN potential calculation. The ground (excited) state energies were obtained in the $12\hbar\Omega$ ($10\hbar\Omega$) model space. Experimental values are from Refs. [32].

^{8}B

	Expt.	CD-Bonn 2000	INOY
$\lvert E_{gs}(2^+1)\rvert$	37.7378(11)	32.284	36.148
$E_x(2^+_1 1)$	0.0	0.0	0.0
$E_x(1^+_1 1)$	0.774(6)	0.804	1.199
$E_x(3^+_1 1)$	2.32(20)	2.977	2.854
$E_x(0^+_1 1)$		2.229	3.853
$E_x(1^+_2 1)$		2.988	4.540
$E_x(2^+_2 1)$		3.824	4.897
$E_x(1^+_3 1)$		4.827	6.459
$E_x(2^+_3 1)$		5.175	5.908
$E_x(4^+_1 1)$		6.482	7.138
$E_x(3^+_2 1)$		7.325	8.572
$E_x(0^+_1 2)$	10.619(9)	10.782	11.926

^{8}Li

	Expt.	CD-Bonn 2000	INOY
$\lvert E_{gs}(2^+1)\rvert$	41.277	35.820	39.938
$E_x(2^+_1 1)$	0.0	0.0	0.0
$E_x(1^+_1 1)$	0.981	0.855	1.264
$E_x(3^+_1 1)$	2.255(3)	3.019	2.871
$E_x(0^+_1 1)$		2.480	4.225
$E_x(1^+_2 1)$	3.21	3.247	4.903
$E_x(2^+_2 1)$		3.977	5.114
$E_x(1^+_3 1)$		5.023	6.758
$E_x(2^+_3 1)$		5.290	6.071
$E_x(4^+_1 1)$	6.53(20)	6.691	7.398
$E_x(3^+_2 1)$		7.570	8.915
$E_x(0^+_1 2)$	10.822	10.898	12.049

TABLE IV: The ^{8}B and ^{8}Li point-proton rms radii (in fm), ground-state quadrupole (in $e$fm^2) and magnetic (in μ_N) moments and M1 transitions (in μ_N^2) obtained within the NCSM for different HO frequencies (given in MeV) and model spaces for the CD-Bonn 2000 and INOY NN potentials. Experimental values are from Refs. [32].

^{8}B

CD-Bonn 2000

$\hbar\Omega$	$N_{\max}$	r_p	Q	μ	B(M1; $1^+ \to 2^+$)
12	6	2.436	+5.218	+1.463	3.498
12	8	2.463	+5.420	+1.455	3.506
12	10	2.487	+5.636	+1.455	3.490
12	12	2.520			
11	6	2.514	+5.525	+1.515	3.491
11	8	2.528	+5.696	+1.501	3.495
11	10	2.542	+5.871	+1.496	3.539
Expt.		2.45(5)	(+)6.83(21)	1.0355(3)	9.1(4.5)

INOY

$\hbar\Omega$	$N_{\max}$	r_p	Q	μ	B(M1; $1^+ \to 2^+$)
16	6	2.199	+4.049	+1.192	3.669
16	8	2.241	+4.306	+1.207	3.669
16	10	2.277	+4.580	+1.227	3.649
16	12	2.317			
15	6	2.241	+4.242	+1.238	3.681
15	8	2.276	+4.468	+1.244	3.684
15	10	2.305	+4.710	+1.257	3.667
14	6	2.291	+4.467	+1.288	3.696
14	8	2.318	+4.660	+1.286	3.702
14	10	2.340	+4.867	+1.291	3.688
Expt.		2.45(5)	(+)6.83(21)	1.0355(3)	9.1(4.5)

^{8}Li

CD-Bonn 2000

$\hbar\Omega$	$N_{\max}$	r_p	Q	μ	B(M1; $1^+ \to 2^+$)

12	6	2.139	+2.588	+1.238	4.454
12	8	2.139	+2.690	+1.243	4.428
12	10	2.145	+2.784	+1.241	4.393
12	12	2.161			
Expt.		2.26(2)	+3.27(6)	+1.654	5.01(1.61)
			INOY		
$\hbar\Omega$	$N_{\max}$	$r_{\rm p}$	Q	μ	B(M1; $1^+ \to 2^+$)
16	6	1.938	+2.279	+1.469	4.635
16	8	1.956	+2.377	+1.456	4.610
16	10	1.972	+2.477	+1.439	4.578
16	12	1.991			
Expt.		2.26(2)	+3.27(6)	+1.654	5.01(1.61)

TABLE V: The $\langle {}^8{\rm B}(2^+_{\rm gs})|{}^7{\rm Be}(I^\pi_1)+{\rm p}(l,j)\rangle$ spectroscopic factors obtained within the NCSM for different HO frequencies and model spaces for the CD-Bonn 2000 and INOY NN potentials.

CD-Bonn 2000		^{7}Be+p $I^\pi_1(l,j)$		
$\hbar\Omega$ [MeV]	$N_{\max}$	$\frac{3}{2}^-(1,\frac{3}{2})$	$\frac{3}{2}^-(1,\frac{1}{2})$	$\frac{1}{2}^-(1,\frac{3}{2})$
11	6	0.977	0.120	0.285
11	8	0.967	0.116	0.280
11	10	0.959	0.111	0.275
12	6	0.978	0.107	0.287
12	8	0.969	0.103	0.281
12	10	0.960	0.102	0.276
14	6	0.979	0.086	0.288
14	8	0.967	0.085	0.284
14	10	0.958	0.085	0.280
INOY		^{7}Be+p $I^\pi_1(l,j)$		
$\hbar\Omega$ [MeV]	$N_{\max}$	$\frac{3}{2}^-(1,\frac{3}{2})$	$\frac{3}{2}^-(1,\frac{1}{2})$	$\frac{1}{2}^-(1,\frac{3}{2})$
14	6	0.987	0.074	0.283
14	8	0.976	0.072	0.277
14	10	0.966	0.072	0.272
16	6	0.988	0.060	0.281
16	8	0.977	0.061	0.276
16	10	0.965	0.063	0.271

TABLE VI: Parameters of the Woods-Saxon potentials obtained in the fits to the interior part of the NCSM $\langle {}^8{\rm B}(2^+_{\rm gs})|{}^7{\rm Be}(I^\pi_1)+{\rm p}(l,j)\rangle(r)$ overlap functions under the constraint to reproduce experimental separation energies. The p-wave channels for the ^{7}Be ground and the first excited state are shown. Results for the $10\hbar\Omega$ model space and HO frequencies of $\hbar\Omega = 12(14)$ MeV for the CD-Bonn 2000 (INOY) NN potential. Woods-Saxon potential parameters from Ref.[38] (with slight modification of V_0) that we use for the scattering states are also shown.

CD-Bonn 2000 $10\hbar\Omega$ $\hbar\Omega = 12$ MeV							
$I^\pi_1(l,j)$	V_0	R_0	a_0	$V_{\rm ls}$	$R_{\rm ls}$	$a_{\rm ls}$	$R_{\rm C}$
$\frac{3}{2}^-(1,\frac{3}{2})$	-51.037	2.198	0.602	-9.719	2.964	0.279	2.198
$\frac{3}{2}^-(1,\frac{1}{2})$	-45.406	2.613	0.631	-8.414	2.243	0.366	2.613
$\frac{1}{2}^-(1,\frac{3}{2})$	-49.814	2.235	0.553	-17.024	3.080	0.338	2.235
INOY $10\hbar\Omega$ $\hbar\Omega = 14$ MeV							
$I^\pi_1(l,j)$	V_0	R_0	a_0	$V_{\rm ls}$	$R_{\rm ls}$	$a_{\rm ls}$	$R_{\rm C}$
$\frac{3}{2}^-(1,\frac{3}{2})$	-58.836	2.052	0.561	-7.518	2.768	0.253	2.052
$\frac{3}{2}^-(1,\frac{1}{2})$	-55.924	2.470	0.580	-17.454	2.027	0.429	2.470
$\frac{1}{2}^-(1,\frac{3}{2})$	-44.300	2.455	0.509	-13.325	1.011	0.347	2.455
scattering state							
	V_0	R_0	a_0	$V_{\rm ls}$	$R_{\rm ls}$	$a_{\rm ls}$	$R_{\rm C}$
	-42.2	2.391	0.52	-9.244	2.391	0.52	2.391

TABLE VII: Cross sections for the proton-removal reactions ${}^8{\rm B} + {}^9{\rm Be}$ at 41 MeV/nucleon (MSU) and ${}^8{\rm B} + {}^{12}{\rm C}$ at 936 MeV/nucleon (GSI). The calculated total inclusive cross sections are given by $\sigma_{\rm inc}^{\rm (th-B)}$ for the CD-Bonn 2000 interaction and $\sigma_{\rm inc}^{\rm (th-I)}$ for the INOY interaction. The $10\hbar\Omega$ model space and HO frequencies of 12(16) MeV were employed for the CD-Bonn 2000 (INOY). The calculated cross sections for the excited state are given by $\sigma_{\rm exc}^{\rm (th-B)}$ and $\sigma_{\rm exc}^{\rm (th-I)}$, respectively.

	$\sigma_{\rm inc}^{\rm (exp)}$ [mb]	$\sigma_{\rm inc}^{\rm (th-B)}$ [mb]	$\sigma_{\rm inc}^{\rm (th-I)}$ [mb]	$\sigma_{\rm exc}^{\rm (exp)}$ [mb]	$\sigma_{\rm exc}^{\rm (th-B)}$ [mb]	$\sigma_{\rm exc}^{\rm (th-I)}$ [mb]
MSU	–	82.96	71.85	–	15.31	13.26
GSI	94 ± 9	99.66	82.93	12 ± 3	16.36	13.17

TABLE VIII: The calculated ^{7}Be(p,γ)^{8}B S-factor, in eV b, at the energy of 10 keV. Two ways of correcting the NCSM overlap asymptotics, by the Woods-Saxon potential solution fit (WS) and by a direct Whittaker function matching (Whitt), are compared. The asymptotic normalization constants, in fm$^{-1/2}$, correspond to the Whittaker function matching case. Results obtained using the CD-Bonn 2000 and INOY NN potentials at different HO frequencies and model spaces as well as the S_{17} extrapolated values with their estimated errors are presented.

CD-Bonn 2000					
$\hbar\Omega$ [MeV]	$N_{\max}$	$C_{1,3/2}$	$C_{1,1/2}$	$S_{17}^{\rm Whitt}$	$S_{17}^{\rm WS}$
15	6	0.647	0.195	16.81	17.80
15	8	0.660	0.206	17.58	18.87
15	10	0.672	0.216	18.33	19.81
14	10	0.680	0.220	18.78	20.21
13	10	0.692	0.234	19.64	21.02
12	6	0.693	0.240	19.75	21.24
12	8	0.696	0.242	19.96	21.14
12	10	0.704	0.247	20.45	21.66
11	6	0.715	0.261	21.30	22.38
11	8	0.715	0.263	21.33	23.04
11	10	0.720	0.262	21.60	23.06
NCSM S_{17}(10 keV)					22.1 ± 1.0
INOY					
$\hbar\Omega$ [MeV]	$N_{\max}$	$C_{1,3/2}$	$C_{1,1/2}$	$S_{17}^{\rm Whitt}$	$S_{17}^{\rm WS}$
16	10	0.641	0.182	16.34	17.49
15	10	0.649	0.189	16.83	17.95
14	6	0.652	0.190	16.94	17.78
14	8	0.654	0.194	17.12	18.21
14	10	0.660	0.198	17.44	18.46
NCSM S_{17}(10 keV)					19.0 ± 1.0